EUMETSAT

esa

MONITORING VOLCANIC ASH FROM SPACE

ESA-EUMETSAT workshop on the 14 April to 23 May 2010 eruption at the Eyjafjöll volcano, South Iceland

C. ZEHNER (Editor)
ESA/ESRIN

Ash-rich and collapsing phreatomagmatic eruption column at 18:32 on 16 April seen from Skógar; view is to the Northwest. Photograph taken by Ármann Höskuldsson

3. What are the observations VAACs need and what are the implications for future satellite observing systems (e.g. METOP, MTG, post-EPS, ADM, Earthcare, Sentinels)?

Lead authors: A.J. Prata, Aminou D., Buongiorno F., Carboni E., Fehr T., Mannstein H., Munro R., Remedios J., and Thorsteinsson H.

3.1 VAAC Requirements and the Ash Concentration Threshold

Satellite data can be used in a variety of ways to assist with Volcanic Ash Advisory Centre (VAAC) operations. Prata and Tupper (2009) have recently summarised the status of the science surrounding ash identification from satellites and the aviation problem in a *Special Issue* of *Natural Hazards*. Papers within this issue go into the details of the various techniques and research areas contributing to VAAC operations. Table 2 shows some of the requirements and parameters identified as potentially measurable from satellites.

VAACs operate under the auspices of ICAO and most are collocated with Meteorological Watch Offices (MWOs) within operational meteorological centres. MWOs immediately advise VAACs when a volcanic eruption occurs and request a series of actions and advice from the VAAC. This advice includes ash advisories in text and optionally in a graphical format. By international agreement, the current system does not require graphics in the form of ash concentration plots. Most VAACs have the capability to run sophisticated atmospheric dispersion models and these are used to provide forecasts of the movement and position of volcanic ash clouds at agreed time-steps, typically with a 6 h forecast time interval.

Requirement	Parameters
Operational data provision	- Standardised Volcanic ash product - Real-time - Nowcasting - Transmission in real-time - Timing (5 min warning)
Repetition rate	- 15 mins or better
Data Latency	
Early Warning	- Gas Emissions (SO_2, CO_2, HCl, HF) - Deformation - Hot Spot detection
Detection	- Ash/no-ash and/or SO_2 - Quantitative Estimation
Source parameters, ESP	- Real-Time information - Size distribution (particle effective radius, shape) - Mass flux - Water vapour and temperature profile
Validation	- Dispersion models - Spatial dimension - Concentration - Size distribution - SO_2 and/or ash
End of Eruption	

Table 2. VAAC requirements and associated parameters that could be measured by satellite instruments.

Generation of the ash advisories requires use of as much information as possible from diverse sources, including and probably most importantly, from satellite instruments. Information from ground-based observers, pilots, and from volcanological observatories are also vital in developing the ash advisory. Here we concentrate on the use of satellite data.

Almost universally all VAACs rely heavily on access to real-time satellite imagery to identify and locate volcanic clouds. The primary kind of data used are images, visible and infrared, with animation if available. Interpreting these data requires a high degree of meterological skill and training. Good observational meteorologists are able to use context and experience to identify and interpret volcanic features within satellite images. At this stage of analysis the interpretation must be done rapidly and is often subjective, depending on exactly what data are available (e.g. rapid scan geosynchronous data or less frequent polar orbiting data). Locations of volcanic features within images are compared with the output of dispersion models and an estimate of the extent and location of the volcanic hazard is made. The feature is defined by a polygon with a small number of sides and typically three height intervals are specified. Often it is possible to subjectively utilise the model trajectory with the information from the satellite image to estimate the vertical layer of the atmosphere most affected. However, when there is no wind shear or winds blowing in similar directions and speeds but at different heights, the height identification can be ambiguous. At many VAACs the use of satellite data stops at this point. Some VAACs can go further by using cloud shadows in visible imagery to estimate volcanic cloud heights, or use thermal images to determine cloud top temperatures that can be interpreted to cloud top heights by use of a nearby contemporaneous radiosounding. Very few VAACs make use of any satellite data in their operations, other than geosynchronous meteorological imagery (e.g. SEVIRI, GOES and MTSAT) and polar orbiting operational sensors, such as the NOAA/AVHRRs. These data are images; at most the only quantitative processing done is to convert the thermal imagery into brightness temperatures. For VAACs that do make use of the thermal brightness temperatures, the brightness temperature difference image (BTD) based on the 'reverse absorption' effect (Prata, 1989a, b) at 11 and 12 µm (sometimes referred to as the 'split-window'), are found to be particularly useful for identifying ash. Table 3 lists some of the methods used to detect ash from current satellites.

In Europe, EUMETSAT have provided a 'dust' RGB composite image based on imagery with channels centred at 8.6, 10.8 and 12 µm. This RGB imagery has proved very useful for identifying volcanic clouds, but it does not discriminate between ash and SO_2 (the channel at 8.6 µm is affected by SO_2 absorption). Also, to untrained users, the imagery can be confusing and a high reliance must be placed on context and movement in the images to properly identify volcanic features. Nevertheless, these RGB composites are now widely used and have proved helpful.

Name	Principle	Reference
RA	2-band IR (11 and 12 µm)	Prata (1989a,b)
Ratio	2-band IR (11 and 12 µm)	Holasek and Rose (1991)
4-band	IR + visible	Mosher (2000)
TVAP	3-band IR (3.9, 11 and 12 µm)	Elrod et al. (2003)
PCI	Multi-band principle components	Hilger and Clark (2002a,b)
WVC	2-band IR + water vapour correction	Yu et al. (2002)
RAT	3-band IR (3.9, 11 and 12 µm)	Pergola et al. (2004)
3-band	3-band (IR + visible)	Pavalonis et al. (2006)

Table 3. The main satellite based methods for detecting and discriminating volcanic ash clouds.

RA=Reverse Absorption; TVAP=Three band Volcanic Ash Product; PCI=Principle Components; RAT=Robust AVHRR Technique; WVC= Water Vapour Correction method.

VAAC	GEO Satellite(s)	Temporal Refresh	Spectral Capabilities	Next Generation GEO Satellite
Anchorage	GOES-11	30 minutes	Split-window	GOES-R (2015)
Buenos Aires	GOES-12 GOES-13 MSG	15 minutes 180 minutes 15 minutes	No split-window No split-window Advanced	GOES-R (2015)
Darwin	MTSAT FY2D FY2E	60 minutes 60 minutes 60 minutes	Split-window Split-window Split-window	GOES-R like from JMA (2020?) and **FY4A from China (2014)**
London	MSG	15 minutes	Advanced	**MTG (~2018)**
Montreal	GOES-11 GOES-13	30 minutes 15 or 30 minutes	Split-window No split-window	GOES-R (2015)
Tokyo	MTSAT FY2D FY2E	30 minutes 60 minutes 60 minutes	Split-window Split-window Split-window	GOES-R like from JMA (2020?) and **FY4A from China (2014)**
Toulouse	MSG	5 or 15 minutes	Advanced	**MTG (~2018)**
Washington	GOES-11 GOES-12 GOES-13 MSG	30 minutes 15 minutes 15 or 30 minutes 15 minutes	Split-window No split-window No split-window Advanced	GOES-R (2015)
Wellington	MTSAT GOES-11	60 minutes 180 minutes	Split-window Split-window	GOES-R like from JMA (2020?) and GOES-R (2015)

Table 4: An overview of the geostationary satellite capabilities is shown as a function of VAAC. The table summarises the temporal and spectral capabilities (those relevant to volcanic ash remote sensing) of each instrument that covers each VAAC area of responsibility. In addition, future geostationary satellite capabilities are summarised. Next generation satellites that include a hyperspectral sounding capability are shown in bold.

In the last 3 years or so, data from research satellites have become increasingly available within a time-frame that is useful for VAAC procedures. For example, OMI and GOME-2 SO_2 data products can be accessed via web pages and these are found to be very helpful in identifying volcanic clouds, because measuring SO_2 from space is much easier than identifying ash, which is the major hazard to aviation. SO_2 and ash do not always travel together and on occasion little SO_2 is emitted by a volcano making the use of SO_2 as a proxy for ash, problematic. Table 4 shows the current and near future satellite capabilities available to VAACs.

Annex 3a shows some example satellite images of volcanic ash clouds, SO_2 and the aerosol index, a measure of absorption of UV light by particles.

Prior to 21 April 2010, all VAACs provided ash advisories without the need to quantify the amount or concentration of ash. Advice was given based upon the observation of ash in the atmosphere, and subsequent modeling based on a standard volcanic source strength, dispersed by measured winds. Thus there was no requirement for quantitative volcanic ash products from satellite data, although much research had been done on this topic and many such products were available to the research community. A new limit was imposed at a level of 2 mgm^{-3}, for which areas identified with levels exceeding this would be deemed a "no fly zone". This new limit is only applicable for eruptions within the jurisdiction of the London VAAC and no such limit has been sanctioned by ICAO. It is unclear whether the limit will be accepted throughout the nine VAAC regions, or indeed whether this limit will be increased or decreased after review.

The imposition of a limit implies that the dispersion model is capable of providing a contour showing ash concentrations and in particular that a level of 2 mgm^{-3} can be delineated. In order to be able to do this, accurate information on the volcanic source (e.g. the mass flux, vertical distribution of mass, the column height and the particle size distribution) is needed.

Generally this kind of information is not readily available even at the most advanced and well-instrumented volcano observatories. Without the volcano source information the only other means to constrain the dispersion model concentrations is through direct measurement. Downwind measurements of the plume concentration can be made using ground-based, balloon-borne, airborne and satellite-based instruments.

3.2 Infrared satellite measurements

Satellite measurements of ash mass loadings are currently available from instruments on board both polar orbiting and geosynchronous platforms. Notably among these for Europe are: AVHRR, (A)ATSR, SEVIRI, AIRS and IASI. These instruments have thermal channels at 11 and 12 µm necessary to detect and quantify volcanic ash. It is not at all a difficult goal to detect mass loading of 2 gm^{-2}, which translates to an ash concentration of 2 mgm^{-3} for an ash layer of 1 km thickness. The reverse absorption method is described in Annex 3b and an example is shown on the sensitivity of the method to ash concentrations of 2 mgm^{-3}.

Horizontal resolution can be an issue but generally speaking the spatial resolution of most of today's operational and research satellite instruments are sufficient for detecting most hazardous volcanic clouds. Horizontal resolutions of 1–10 km are adequate. Vertical resolution is important but most satellite instruments can only provide column estimates. This appears to be a large gap in the capability of current satellite instruments to address the volcanic ash problem.

IRS spectral range should be extended to provide coverage of SO_2 features to add night-time SO_2 observation capability from GEO.

3.3 UV and Visible light measurements from satellites

Other current satellite instruments can be used to provide validation of some of the parameters required for accurate retrieval of ash mass loadings, but it is necessary to be clear which satellite data are of primary importance and which are secondary. Most of the instruments using visible radiation as a source are of secondary importance for two reasons. First, these instruments can only measure when the Sun is above the horizon and therefore cannot be used in an operational volcanic ash hazard identification system. Second, these instruments are not optimised for measuring the 1–10 µm sized particles responsible for causing engine damage in commercial jets. However, they are capable in some cases of providing cloud top heights and can provide aerosol optical depth measurements, which may be used for validation.

Because of the nature of volcanic activity (unpredictable, sporadic and often in remote locations) it is easy to see the importance of satellite measurements. VAACs require near continuous observations and require data in a rapid manner. Summarising these points for the UV/VIS sensors:

(1) geosynchronous observations are to be preferred, but full disk coverage is important to provide information for the full area covered by the London and Toulouse VAACs

(2) spatial resolution should be as good as possible also for the LEO instruments e.g. GOME-2 (the current safety margin is 60 km which is smaller than the current GOME-2 ground pixel)

(3) data access should be fast and easy also for ESA/EUMETSAT missions/ instruments

(4) VAACs are concerned with ash that is not a standard product from UV/VIS sensors. However, SO_2 is useful as its identification is fast and unambiguous and because often SO_2 emissions precede eruptions. The absorbing index (AI) type products which are produced from UV/VIS are qualitative but fast and much less affected by clouds as current ash products from imagers.

(5) UV/VIS data should not be ignored as it can provide rapid and easy to interpret information on volcanic eruptions

3.4 Pre-cursor and Early Warnings

Early warning and early readiness in the event of an eruption will rely on the expertise and active involvement of volcanic observatories. Seismicity, seismic mapping, crustal deformation and gaseous release are only a few types of observations that help observatories to prepare the operational community for the onset of an ash eruption. Increased density of ground sensors in the vicinity of volcanoes will help researchers to better map and understand their volcanoes.

Remote sensing with interferometric SAR (InSAR) observations (eg. ENVISAT-ASAR, Terra-SAR/TanDEM-X, Radarsat) has also revolutionised the detection of ground deformation. InSAR observations are today an important and accepted tool in the early detection of magma injection and in mapping the underlying structure of a volcano. A policy of regular (weekly/monthly) and openly available InSAR observations of volcanoes will greatly aid our understanding of eruptions.

Remote sensing of thermal anomalies, especially in the SWIR, can give signs of an impending eruption as well as serving as a negative plume indicator (optically thin source). Volcanologists have expressed that higher spatial resolution in thermal imaging will be an important future improvement.

The majority of volcano observatories and the International Civil Aviation Organization have a relatively simple and straightforward system of four levels increasing from ‘non-eruptive’ (usually green or white), through ‘elevated unrest’ (yellow), ‘heightened unrest’ (orange) to ‘eruption underway’ (red).

These stages of disaster management are most useful for disaster managers but volcano observatories tend to structure the evolving stages of their requirements slightly differently, thus three observation scenarios can be distinguished:

— Identification of phenomena

  Locating and identifying potentially hazardous or important features such as fumaroles, lava domes, lava flows, crater lakes and establishing ‘background’ levels of activity.

— Monitor expansion/development of phenomena

  Collection of a time series of data that chronicles changing levels of activity from background to hazardous levels. Time frames for such monitoring vary widely from days to years. Such data can help in modelling possible impacts of future hazardous events.

— Generation of hazards

  Locating where hazards are being generated and areas impacted and likely to be impacted can help with search and rescue or damage assessment. Impacts and extents are essential to understand major events – often close access is impossible during or shortly after major volcanic events. Data can be used to improve future models of hazards and their impacts.

Ash clouds are generated by explosive volcanic eruptions, in order to mitigate the volcanic risk and therefore increase the preparedness for a possible volcanic event, satellite systems should be equipped with suitable instrumentation to support the monitoring of precursors especially for volcanoes which lack of adequate ground monitoring systems.

To accomplish these tasks the current planned missions should be integrated with instruments that may furnish, by means of systematic observations, information on the variation of key volcanic parameters:

(1) thermal anomalies detection and analysis in the pre-eruptive periods

(2) changes in gas emission composition and volcanic aerosol concentrations in permanent degassing plumes from summit craters or fumaroles fields

(3) deformation of the surface by means of SAR images and GPS

Focusing on point 1 and 2 Table 5 summarises the observational objectives and the related measurements.

Objective	Related Quantitative Measures
Correlation between **thermal precursors and eruptive activity**	· **% of thermal anomalies that precede eruptions** as a function of anomaly area and intensity, for a given volcano · **Rate of increase/decrease of anomaly intensity/ flux** as a function of eruption duration/volume/flux
Correlation between gas emissions from permanent degassing plumes (summit craters and fumarole fields) and volcanic eruptive activity	· **Rate of increase/decrease of SO_2, CO_2, H_2O** (primarily) **concentration /flux** in pre-eruptive periods and during eruptive activity
Correlation between volcanic aerosols from permanent degassing plumes (summit craters and fumaroles fields) and volcanic ash plumes emitted during the eruptive activity	· **Changes in the aerosol concentrations** in pre-eruptive periods, AOT variation in function of time
Temporal, spatial, energetic, and instrumental **limits on remote thermal anomaly detection**	· **Required sampling frequency** for >90% detection certainty as a function of anomaly intensity, instrumental resolution, and **$NE\Delta T_I$ (instrumental)**
Sensitivity of **detection thresholds to intrinsic and extrinsic** variables	· **$NE\Delta T_x$ (scene noise relative to the anomaly)** as a function of scene roughness, roughness, topography, temperature, emissivity, atmospheric water vapor, cloud cover, volcanogenic emissions, seasonal variables
Global Thermal Anomaly Catalog **(GTAC)**	· **GIS locations of anomalous pixels** as a function of time referenced by radiant intensity and/or T at the surface (atmospherically corrected/T/E-separated) or at the instrument.
Systematic **surveys of all eruptions**	· **Time-series distribution of radiant intensity/ flux** of thermal anomalies as a function of time/ distance from the eruption apex and/or vent.

Table 5: Volcanic precursor observation objectives and measurements

Satellite - Sensor	TIR Spatial Resolution	Night/Day	Revisiting Time	# TIR bands	SWIR bands
MSG – SEVIRI	3 to 5 km	D,N	Geostationary (15 min)	5	1
NOAA - AVHRR	1.1 km	D,N	12 hr	2	1
METOP - AVHRR-3	1.1 km	D,N	Daily	2	1
TERRA, AQUA - MODIS	1.1 km	D,N	Daily	10	4
ERS1 – ATSR ERS2 – ATSR-2	1 km	D,N	3 to 5 days	2	1
ENVISAT - AATSR	1 km	D,N	3 to 5 days	2	1
LANDSAT - TM / ETM	120m / 60m	D, [N]	16 days	1	2
TERRA - ASTER	90m	D	16 days	5	6
SENTINEL-2 MSI	30-60 m	D [N]	5 day (2 satellites)	0	3
SENTINEL-3 -SLST	500-1km	D,N	2 days (2 satellites)	2	3

Table 6: Sensors, resolutions, revisit times and bands available from current and some proposed satellite instruments useful for early warning/precursors.

3.5 Sensor requirements for precursor/early warnings

The current missions and the near-future missions (ESA/EUMETSAT - SENTINELS) will ensure the observation with a high repetition cycle both for observing lava flows (SWIR/MIR) and ash clouds (TIR) events (see Table 6). Nevertheless it is obvious that there is an observational gap for TIR/MIR multispectral sensors at high spatial resolution which are needed to locate the specific thermal anomalies and small gas emissions to monitor the pre-eruptive phases of volcanoes.

A specific goal could be achieved by combining future systems (Sentinels) with high spectral capabilities (sounders, spectrometers) and high global coverage (geosynchronous) with polar orbiting systems with a repetition cycle between 3-16 days (systematic acquisitions not on demand) and spatial resolution between 30-60 m. Spectral coverage could be a select number of spectral channels suitable for volcanic observations. The available detector technology and payload design may permit development of a class of small sensors that may fly in missions that are already scheduled.

3.6 Global and Regional Systems

It is worth reflecting on the fact that many of the already highlighted limitations in ash aerosol observations, such as obscuring clouds and a lack of direct measurements, are in fact very common limitations within meteorology and Earth Observations in general. The May 26/27 meeting at ESRIN has highlighted the importance for diversity in observations and focus. Gaps in observations of the atmosphere are a reality that we must learn to deal with by thinking big.

Meteorological organizations have long since recognized the importance of sharing data and to work together through comprehensive networks of weather observations, common standards and some times common processing facilities. International bodies such as the WMO, EUMETNET, ICAO and EUMETSAT are instrumental in uniting countries in their effort to share data in monitoring of the atmosphere. It is also natural that these bodies take it onto themselves to establish and to improve standards and guidelines on ash.

Ultimately we want to realize a comprehensive observation system with the ability to detect ash in multiple Earth locations and under varied atmospheric conditions. At the same time we also need the ability to share data and products

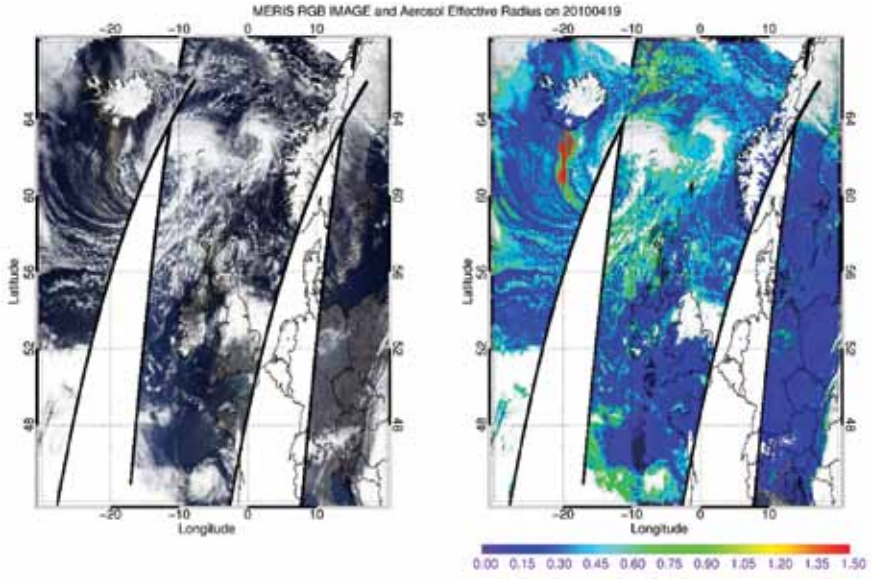

Fig 8. The Red-Green-Blue composite image (left) shows the ash plume from Iceland's Eyjafjoll volcano and clouds, as seen by Envisat's Medium Resolution Imaging Spectrometer (MERIS) on 19 April 2010. The right image shows the retrieved aerosol effective radius (indicating the ash cloud in red). Credits: W. von Hoyningen-Huene

effectively and in a timely manner. To ensure good progress, meteorology, volcanology and the satellite agencies will need to establish a formal forum to interact on a broad range of topics, ranging from ground instrument financing to data access policies and standards. Long-established international cooperations on a broad range of observations within meteorology should give us good hope of succeeding.

A comprehensive operational observation system for ash needs to combine both geostationary and polar orbiting observatories. It would therefore be most advantageous if detailed sensitivity to ash aerosol was to be made an official specification in future meteorological satellite sensors.

Conclusions

— The combination of ash load (and concentration) derived from IASI, AIRS and other instruments with a high spectral resolution in the thermal IR in combination with the VA detection and tracking in SEVIRI is a promising technique for ash cloud monitoring. It would provide quantitative information in a way which allows to monitor ash clouds and SO_2 with a high temporal resolution in a now-casting mode day and night.

— The operational meteorological satellites (MTP) will provide these capabilities also in future (Annex 3c). Nevertheless, it is important to **validate** the derived quantitative observations **by in situ measurements**. Due to the change of zero tolerance to an ash threshold value the validation became more important then before.

— For future systems the possibility of direct assimilation of radiances into weather forecast models should be kept in mind.

— Two primary ESA satellite missions (EarthCare and ADM-Aeolus) are likely to contribute useful information for monitoring ash clouds. These are described in Annex 3c and a list of future systems useful for the ash problem is provided in Table 3c1 of Annex 3c.

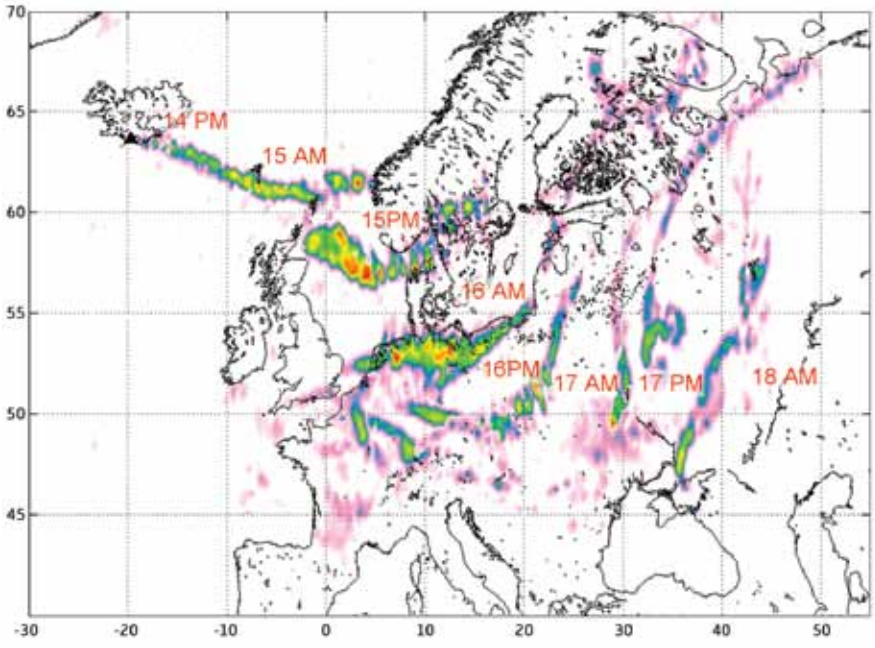

Fig 9. Integrated plot of the Infrared Atmospheric Sounding Interferometer (IASI) ash radiance index for 14-18 April 2010. The overpass times are around 9.30 AM and 9.30 PM.
Credits: L. Clarisse, ULB

3.7 Future Missions Needed

Geostationary imagery and sounding from UV to TIR (like MTG), polar orbiting scanning LIDARs (future), and polar orbiting stereo-viewing imagers (like MISR) are the optimum combination to retrieve ash clouds from space.

Nevertheless such an optimal satellite observing system will be only one component of a global end-to-end monitoring/forecasting system, that will also include ground-based measurements (e.g. LIDAR, Radar, ceilometers, radiometers), airborne measurements, and several operational and R&D modelling capabilities worldwide.

Annex 3a shows some examples of current satellite data that are capable of observing ash clouds. These examples have been chosen because the data identify volcanic substances (either ash or SO_2) as opposed to aerosols (e.g. AOD).

References

Barton IJ, Prata AJ, Watterson IG, Young SA (1992) Identification of the Mount Hudson volcanic cloud over SE Australia. Geophys Res Lett 19:1211–1214

Bernard A, Rose WI (1984) The injection of sulfuric acid aerosols in the stratosphere by the El Chichon volcano and its related hazards to the international air traffic. Nat Hazards 3(1):59–67. doi:10.1007/ BF00144974

Bluth GJS, Schnetzler CC, Krueger AJ, Walter LS (1993) The contribution of explosive volcanism to global atmospheric sulphur dioxide concentrations. Nature 366:327–329

Carn SA, Krueger AJ, Krotkov NA, Gray MA (2004) Fire at Iraqi sulfur plant emits SO_2 clouds detected by Earth Probe TOMS. Geophys Res Lett 31:L19105. doi:10.1029/2004GL020719

Carn SA, Krotkov NA, Yang K, Hoff RM, Prata AJ, Krueger AJ, Loughlin SC, Levelt PF (2007) Extended observations of volcanic SO_2 and sulphate aerosol in the stratosphere. Atmos Chem Phys Discuss 7:2857–2871

Carn SA, Prata AJ, Karlsdottir S (2008) Circumpolar transport of a volcanic cloud from Hekla (Iceland). J Geophys Res 113. doi:10.1029/2008JD009878

Casadevall TJ (1994) The 1989/1990 eruption of Redoubt Volcano Alaska: impacts on aircraft operations. J Volcanol Geotherm Res 62(30):301–316

Casadevall TJ, Delos Reyes PJ, Schneider DJ (1996) The 1991 Pinatubo eruptions and their effects on aircraft operations. In: Newhall CG, Punongbayan RS (eds) Fire and mud: eruptions and lahars of Mount Pinatubo, Philippines. Philippines Institute of Volcanology and Seismology, Quezon City, University of Washington Press, Seattle, pp 625–636

Clerbaux C, Hadji-Lazaro J, Turquety S, George M, Coheur P-F, Hurtmans D, Wespes C, Herbin H, Blumstein D, Tournier B, Phulpin T (2007) The IASI/MetOp I mission: first observations and high- lights of its potential contribution to GMES. COSPAR Inf Bull 2007:19–24

Constantine EK, Bluth GJS, Rose WI (2000) TOMS and AVHRR sensors applied to drifting volcanic clouds from the august 1991 eruptions of Cerro Hudson. In: Mouginis-Mark P, Crisp J, Fink J (eds) AGU Monograph 116—Remote Sensing of Active Volcanism, pp 45–64

Eckhardt S, Prata AJ, Seibert P, Steibel K, Stohl A (2008) Estimation of the vertical profile of sulfur dioxide injection into the atmosphere by a volcanic eruption using satellite column measurements and inverse transport modeling. Atmos Chem Phys Discuss 8:3761–3805

Eisinger M, Burrows JP (1998) Tropospheric sulfur dioxide observed by the ERS-2 GOME instrument. Geophys Res Lett 25(22):4177–4180

Ellrod GP, Connell BH, Hillger DW (2003) Improved detection of airborne volcanic ash using multispectral infrared satellite data. J Geophys Res 108(D12):4356. doi:10.1029/2002JD002802

Fleming EL, Chandra S, Shoeberl MR, Barnett JJ (1988) Monthly mean global climatology of temperature, wind, geopotential height and pressure for 0–120 km. National Aeronautics and Space Administration, Technical Memorandum 100697, Washington, DC

Guffanti M, Albersheim S (2008) The United States national volcanic ash operations plan for aviation. Nat Hazards Special Issue: Aviation hazards from volcanoes. doi:10.1007/ s11069-008-9247-1

Hanstrum BN, Watson AS (1983) A case study of two eruptions of Mount Galunggung and an investigation of volcanic eruption cloud characteristics using remote sensing techniques. Aust Meteorol Mag 31:131–177

Hillger DW, Clark JD (2002a) Principal component image analysis of MODIS for volcanic ash. Part I: most important bands and implications for future GOES imagers. J Appl Meteorol 41:985–1001

Hillger DW, Clark JD (2002b) Principal component image analysis of MODIS for volcanic ash. Part II: simulation of current GOES and GOES-M imagers. J Appl Meteorol 41:1003–1010

Holasek RE, Rose WI (1991) Anatomy of 1986 Augustine volcano eruptions as recorded by multispectral images processing of digital AVHRR weather satellite data. Bull Volcanol 53:42–435.

Holasek RE, Woods AW, Self S (1996) Experiments on gas-ash separation processes in volcanic umbrella clouds. J Volcanol Geotherm Res 70:169–181.

Krotkov NA, Carn SA, Krueger AJ, Bhartia PK, Yang K (2006) Band residual difference algorithm for retrieval of SO_2 from the Aura Ozone Monitoring Instrument (OMI). IEEE Trans Geosci Remote Sens 44(5):1259–1266.

Krueger AJ (1983) Sighting of El Chichon sulfur dioxide clouds with the nimbus 7 total ozone mapping spectrometer. Science 220:1377–1379.

Krueger AJ, Walter LS, Bhartia PK, Schnetzler CC, Krotkov NA, Sprod I, Bluth GJS (1995) Volcanic sulfur dioxide measurements from the total ozone mapping spectrometer instruments. J Geophys Res 100(D7):14057–14076.

Krueger AJ, Schaefer SJ, Krotkov N, Bluth GJS, Baker S (2000) Ultraviolet remote sensing of volcanic emissions. In: Mouginis-Marks PJ, Crisp JA, Fink JH (eds) Remote sensing of active volcanism. Geophys Monogr Ser 116:2543, AGU, Washington, DC.

Malingreau J, Kaswanda P (1986) Monitoring volcanic eruptions in Indonesia using weather satellite data: the Colo eruption of July 28, 1983. J Volcanol Geotherm Res 27(1–2):179–194.

Matson M (1984) The 1982 El Chichon volcano eruptions—a satellite perspective. J Volcanol Geotherm Res 23:1–10.

Miller TP, Casadevall TJ (1999) Volcanic ash hazards to aviation. In: Sigurdsson H, Houghton B, McNutt SR, Ryman H, Stix J (eds) Encyclopedia of volcanoes. Academic Press, San Diego, pp 915–930.

Mosher FR (2000) Four channel volcanic ash detection algorithm, Preprint Volume. 10th Conference on Satellite Meteorology and Oceanography, Long Beach, California, 9–14 January, 2000, pp 457–460.

Pavolonis MJ, Feltz WF, Heidinger AK, Gallina GM (2006) A daytime complement to the reverse absorption technique for improved automated detection of volcanic ash. J Atmos Oceanic Technol 23:1422–1444.

Pergola N, Tramutoli V, Marchese F, Scaffidi I, Lacav T (2004) Improving volcanic ash cloud detection by a robust satellite technique. Remote Sens Environ 90:1–22.

Pieri D, Ma C, Simpson JJ, Hufford G, Grindle T, Grove C (2002) Analyses of in-situ airborne ash from the February 2000 eruption of Hekla volcano, Iceland. Geophys Res Lett 29:16. doi:10.1029/2001GL013688.

Prata AJ (1989a) Observations of volcanic ash clouds using AVHRR-2 radiances. Int J Remote Sens 10(4–5):751–761.

Prata AJ (1989b) Radiative transfer calculations for volcanic ash clouds. Geophys Res Lett 16(11): 1293–1296.

Prata AJ, Grant IF (2001) Retrieval of microphysical and morphological properties of volcanic ash plumes from satellite data: application to Mt. Ruapehu, New Zealand. Q J R Meteorol Soc 127(576B): 2153–2179.

Prata AJ, Kerkmann J (2007) Simultaneous retrieval of volcanic ash and SO_2 using MSG-SEVIRI mea- surements. Geophys Res Lett 34:L05813. doi:10.1029/2006GL028691.

Prata AJ, Bluth GJS, Rose WI, Schneider DJ, Tupper AC (2001) Comments on Failures in detecting volcanic ash from a satellite-based technique. Remote Sens Environ 78:341–346.

Prata, A. J., and Tupper, A. T., (2009) Aviation hazards from volcanoes: the state of the science, Nat Hazards doi: 10.1007/s11069-009-9415-y.

Prata AJ, Rose WI, Self S, O'Brien DM (2003) Global, long-term sulphur dioxide measurements from TOVS data: a new tool for studying explosive volcanism and climate. Volcanism and the Earth's atmosphere, geophysics monograph 139 AGU, pp 75–92.

Prata AJ, Carn SA, Stohl A, Kerkmann J (2007) Long range transport and fate of a stratospheric volcanic cloud from Soufriere ills volcano, Montserrat. Atmos Chem Phys 7:5093–5103.

Richardson AJ (1984) El Chichon volcanic ash effects on atmospheric haze measured by NOAA-7 AVHRR data. Remote Sens Environ 16:157–164.

Richter A, Wittrock F, Burrows JP (2006) SO_2 measurements with SCIAMACHY. In: Proceedings of the first conference on atmospheric science, Frascati, Italy, 8–12 May 2006. ESA publication SP-628.

Rose WI, Delene DJ, Schneider DJ, Bluth GJS, Kruger AJ, Sprod I, McKee C, Davies HL, Ernst GJ (1995) Ice in the 1994 Rabaul eruption: implications for volcanic hazard and atmospheric effects. Nature 375:477–479.

Sawada Y (1987) Study on analysis of volcanic eruptions based on eruption cloud image data obtained by the Geostationary Meteorological Satellite (GMS). Technical reports of the Meteorological Research Institute, vol 22, 335 pp.

Sawada Y (1996) Detection of explosive eruptions and regional tracking of volcanic ash clouds with geostationary meteorological satellites (GMS). In: Scarpa R, Tilling RI (eds) Monitoring and miti- gation of volcano hazards. Springer-Verlag, Berlin, Heidelberg, pp 299–314.

Schneider DJ, Rose WI, Kelley L (1995) Tracking of 1992 eruption clouds from Crater Peak of Mount Spurr volcano, Alaska, using AVHRR. US Geol Surv Bull 2139:27–36.

Schneider DJ, Rose WI, Coke LR, Bluth GJS (1999) Early evolution of a stratospheric volcanic eruption cloud as observed with TOMS and AVHRR. J Geophys Res 104(D4):4037–4050.

Simkin T, Seibert L (1994) Volcanoes of the world, 2nd edn. Geoscience Press, Tucson Simpson JJ, Hufford G, Pieri D, Berg J (2000) Failures in detecting volcanic ash from a satellite-based technique. Remote Sens Environ 72:191–217.

Simpson JJ, Hufford G, Pieri D, Servranckx R, Berg J (2002) The february 2001 eruption of Mount Cleveland, Alaska: case study of an aviation hazard. Weather Forecast 17:691–704.

Thomas W, Erbertseder T, Ruppert T, Van Roozendael M, Verdebout J, Balis D, Meleti C, Zerefos C (2004) On the retrieval of volcanic sulfur dioxide emissions from GOME backscatter measurements. J Atmos Chem 50:295–320. doi:10.1007/s10874-005-5079-5.

Torres O, Bhartia PK, Herman JR, Ahmad Z, Gleason J (1998) Derivation of aerosol properties from satellite measurements of backscattered ultraviolet radiation: theoretical basis. J Geophys Res, 103(D14):17099–17110.

Tupper A, Carn SA, Davey J, Kamada Y, Potts RJ, Prata AJ, Tokuno M (2004) An evaluation of volcanic cloud detection techniques during recent significant eruptions in the western ring of fire. Remote Sens Environ., 91:27–46.

Urai M (2004) Sulfur dioxide flux estimation from volcanoes using advanced spaceborne thermal emission and reflection radiometer—a case study of Miyakejima volcano, Japan. J Volcanol Geotherm Res., 134(1–2):1–13.

Van Geffen J, Van Roozendael M, Di Nicolantonio W, Tampellini L, Valks P, Erbetseder T, Van der A (2007) Monitoring of volcanic activity from satellite as part of GSE PROMOTE. Proceedings of the first conference on atmospheric science, Frascati, Italy, 8–12 May 2006. ESA publication SP-628.

Watkin SC (2003) The application of AVHRR data for the detection of volcanic ash in a volcanic ash advisory centre. Meteorol Appl 10:301–311.

Wen S, Rose WI (1994) Retrieval of sizes and total masses of particles in volcanic clouds using AVHRR bands 4 and 5. J Geophys Res 99(D3):5421–5431.

Witham CS, Hort MC, Potts R, Servranckx R, Husson P, Bonnardot F (2007) Comparison of VAAC atmospheric dispersion models using the 1 November 2004 Grimsvtn eruption. Meteorol Appl 14: 27–38.

Yu T, Rose WI, Prata AJ (2002) Atmospheric correction for satellite-based volcanic ash mapping and retrievals using split window IR data from GOES and AVHRR. J Geophys Res 107(D16):4311. doi:10.1029/2001JD000706.

Annex 1d - The role of Ground-Based Meteorological Radars within Volcanic Ash Observation and Monitoring Capability

F. S. Marzano[1], E. Picciotti[2], and G. Vulpiani[3]

[1]Sapienza Univ. of Rome, [2]CETEMPS Univ. of L'Aquila,
[3]Italian Dept. of Civil Protection

Introduction

Volcanic ash is a natural hazard whose effects have been well documented. Volcanic ash is a significant hazard to aircraft operations and the threat to public safety posed by volcanic ashfall at the surface is significant as. Given the significance of the hazards posed by volcanic ash, timely detection and tracking of the ash plume is essential to a successful warning process, particularly during and immediately following an eruptive event.
As pointed out by UK Met Office, *"the largest uncertainty in the ability of numerical models to predict the spread of volcanic ash, and hence to advise aviation regulators, is in observations of the eruption itself: i) Knowing how high the ash is being expelled to; ii) What concentration of ash is being expelled. Current observations, listed by UK Met Office, come from a range of sources: satellite (height & spatial distribution of the main plume), laser cloud base recorders (LCBR) and Light Detection And Ranging (LIDAR) systems (both detecting ash cloud height and depth), seismic (how active is the volcano) and human (height and concentrations)"*. Within this list, the use of **ground-based meteorological microwave radars** should be added whose role, within the volcanic ash monitoring network, is the goal of this contribution.

Remote sensing of ash clouds and ground-based radars

A variety of satellite techniques have been successfully used to track volcanic ash clouds; however, these techniques have certain limitations. As known, these data are subject to limitations in both spatial and temporal resolution. Issues involving the detection of ash clouds using infrared brightness temperature differencing, a commonly used method, have been addressed suggesting several scenarios where effective infrared satellite detection of volcanic ash clouds may be compromised. The brightness temperature differencing, also known as the 'split-window' method, was shown to be subject to errors when the volcanic plume lies over a very cold surface, or when the plume lies above a clear land surface at night where strong surface temperature and moisture inversions exist. Ground-based microwave instrumentation, such as Global Positioning System (GPS) receivers and wind profiler radars, may play a complementary role for monitoring volcanic cloud evolution, even though their operational utility is limited by the relatively small spatial coverage. On the other hand, ground-based LIDAR optical systems may show a higher sensitivity to ash contents with respect to microwave instruments, but counterbalanced by stronger path attenuation effects.
Ground-based microwave radar systems can have a valuable role in volcanic ash cloud monitoring as evidenced by available radar imagery These systems represent one of the best methods for real-time and areal monitoring of a volcano eruption, in terms of its intensity and dynamics. The possibility of monitoring 24 hours a day, in all weather conditions, at a fairly high spatial resolution (less than few hundreds of meters) and every few minutes after and during the eruption is the major advantage of using ground-based microwave

radar systems. They can provide data for determining the ash volume, total mass and height of eruption clouds.
There are still several open issues about microwave weather radar capabilities to detect and quantitatively retrieve ash cloud parameters . A major impairment in the exploitation of microwave weather radars for volcanic eruption monitoring is due to the exclusive use of operational weather radars for clouds and precipitation observation. Several unknowns may also condition the accuracy of radar products, most of them related to microphysical variability of ash clouds due to particle size distribution, shape and dielectric composition. Some of them were analyzed in previous works (Marzano et al., 2005, 2006a) where the sensitivity of microwave radar response to particle ash distribution and wavelength was investigated using ad-hoc physically-oriented random schemes of eruptive ash cloud volumes. Fine-size ash, medium-size ash and lapilli were distinguished with mean diameters of about 0.01, 0.1 and 1 mm, respectively, and concentrations up to few tens of grams per cubic meter. The electromagnetic behavior of pure and porous ash particles was also modeled and its impact on radar reflectivity signature analyzed for fine ash, medium ash and lapilli. No particle aggregation mechanisms and effects were considered in these works.
Indeed, the aggregation of volcanic ash particles within the eruption column of explosive eruptions has been observed at many volcanoes. Recent satellite observations of ash clouds provide strong indirect evidence that ice may be present on ash particles. The aggregation influences the residence time of ash in the atmosphere and the radiative properties of the “umbrella” cloud (i.e. ash at the height of neutral buoyancy spreading in the horizontal and vertical direction). Numerical experiments are helpful to explore processes occurring in the eruption column. Some advanced plume models can simulate the interactions of hydrometeors and volcanic ash, including aggregate particle formation within a rising eruption column (Marzano et al., 2008, 2010b).
In order to quantitatively evaluate the ash retrieval by weather radars, a prototype algorithm for volcanic ash radar retrieval (VARR) has been recently formulated and discussed (Marzano et al., 2006b, 2010b). Starting from measured single-polarization reflectivity, the estimation method is based on two cascade steps: i) a classification of eruption regime and volcanic ash category; ii) estimation of ash concentration and fall rate. Expected accuracy of the VARR algorithm estimates is evaluated on synthetic data sets. A minimum detectable reflectivity analysis is also accomplished for various ash classes and for some available radar systems at S, C and X band.

Sensitivity of ground-based radar to volcanic ash particles

A common question is about the sensitivity of ground-based meteo-radars to volcanic ash particles. Radar systems are thought to be “sensitive to particles above few millimeters such as lapilli and ballistic particles”, a statement which fundamentally incorrect or, at least, incomplete. As shown below, the correct answer should take into account the range distance of the radar antenna from the volcano vent and the acquisition mode as, respectively, received power decreases with the inverse square of the distance and the signal is enhanced if long pulses and space-time averaging is performed.
In order to test ground-based meteorological radar sensitivity, a simplified simulation environment is proposed such that a Gaussian-shaped range profile of volcanic ash concentration has been generated. The radar site has been located in the origin of the system coordinate and the volcanic ash cloud peak has been assumed at a distance d between 30 and 300 km, depending on the pulse repetition frequency (PRF) – note that for PRF=250 Hz, the maximum range r_{max}=600 km, whereas for PRF=2500 Hz it results r_{max}=60 km. The radial resolution has been assumed equal to 300 m (i.e., impulse duration τ=2 μs).

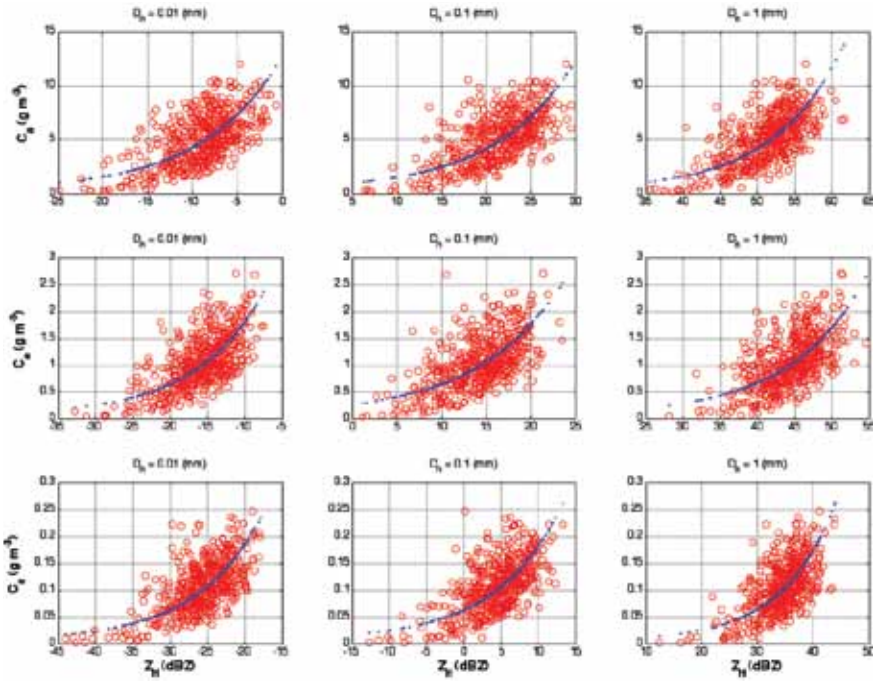

Fig 1d1. Statistical relations between ash concentration Ca and radar reflectivity ZHm for each ash concentration class (intense, moderate and light at upper, middle and lower row panels) and ash size class (fine ash, coarse ash and lapilli at left, middle and right column panels). Regression curves are shown by dotted line (from Marzano et al., 2006b).

A range extension (i.e., standard deviation of the ash Gaussian shape) of 20% of the peak distance has been assumed for every synthetic ash cloud together with a ash concentration random variation having a standard deviation equal to 10% of the maximum value of the ash profile in order to generate concentration range gradients. The choice of a Gaussian-shaped range profile is quite arbitrary, but it is aimed to reproduce scenarios where the ash content decreases from the volcano vent either along a down-wind or up-wind direction, increasing its extension as the ash cloud is advected far from the volcano vent.

The peak concentration of each ash cloud has been set up in order to reproduce the average values of light, moderate and intense concentration classes and distinguishing between fine ash, coarse ash and lapilli. We have defined 3 diameter ash size classes (fine ash, coarse ash and lapilli) and 3 concentration regimes (light, moderate and intense). As a synthesis of available volcanic information, within each class we have supposed a random distribution for: i) *ash particle diameter* with average value equal to 0.01, 0.1 and 1 mm for fine, coarse and lapilli ash ii) *ash concentration* with average equal to 0.1, 1 and 5 g/m^3 for light, moderate and intense concentration regimes. The ash density has been put equal to an average value of 1 g·cm^{-3}. Figure 1d1 depicts the output example of this randomization procedure the for nine ash classes, divided into fine, coarse and gross sizes and light, moderate and intense concentration, in terms of ash concentration C_a versus synthetic measured reflectivity Z_{Hm}.

At all considered frequency bands Rayleigh scattering conditions have been assumed and this implies that radar reflectivity is equal for all the bands (Marzano et al., 2006a). An example of these synthetic ash cloud range profiles is illustrated in Figure 2, where the eruption cloud with a peak at 60 km for all 9 ash average classes is sketched in terms of comparison between the simulated ash-reflectivity response and the Minimum Detectable Z-Reflectivity (MDZ) for the considered radar systems in Table 1 at C and X band (Marzano et al., 2006b).

Some conclusions, constrained to the considered radar systems, can be drawn from this MDZ analysis. i) For C band system, the detection of a fine ash signal larger than MDZ seems to be possible only in case of very *intense* concentration. On the contrary, for coarse and gross ash the radar is able to detect ash particles with reflectivity value larger than zero. ii) For X band radar, there is a lower sensitivity to ash content, fine ash being never detected and coarse detected only if due to a moderate concentration regime. The chosen

Table 1d1 . Three radar systems at S, C and X band and their technical characteristics (from Marzano et al., 2006b)

RADAR SYSTEM CHARACTERISTICS	*Radar S band*	*Radar C-band*	*Radar X-band*
Band	S	C	X
Frequency Range	2.70 – 2.90 GHz	5.45 – 5.82 GHz	9.375 GHz
Transmit Peak Power	600 kW	250 kW	50 kW
RF Pulse Width	0.8 to 2 μs	0.5 to 2 μs	0.5 to 2.0 μs
PRF	250 – 5000 Hz	250 – 2500 Hz	250 – 2500 Hz
Antenna Gain	45 dB	45 dB	41.6 dB
Polarization	Linear H	Linear H	H and V
Half-power Beamwidth	1.0 degree	1.0 degree	1.3 degrees
Sensitivity (MDS)	-113 dBm	-113 dBm	-112 dBm
Receiver Noise Figure	2 dB	2 dB	2.3 dB

X-band system is evidently penalized by characteristics worse than the other two radars (see Table 1d1). iii) For simulations at S band, results are slightly worse than at C band and intermediate with respect to X band. iv) From results with ash cloud peaks at 30, 120 and 240 km, the increase of the range between the radar and ash cloud (from 30 to 240 km) obviously leads to a worse ash sensitivity of microwave radar response. Of course, halving the distance, MDZ is decreased by 6 dB and, by radially averaging reflectivity data, MDZ decreases because the received power is proportional to the impulse duration τ.

Ground-based radar application to volcanic ash monitoring

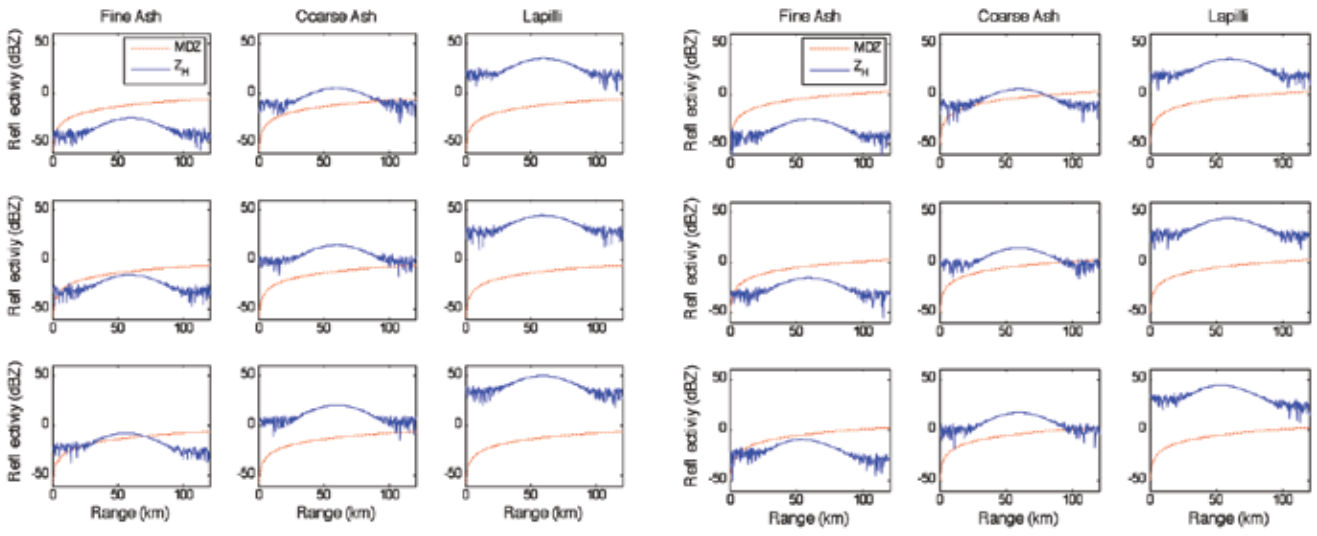

Fig 1d2. (Left) Reflectivity response and minimum detectable reflectivity (MDZ) for ash cloud range profiles with a concentration peak at 60 km at C for a light (top row), moderate (middle row) and intense (bottom row) concentration and fine (left column), coarse (middle column) and lapilli (right column) ash size classes. (Right) Same as in left, but at X band (from Marzano et al., 2006b).

The potential of radar data in observing volcanic ash clouds, has been analyzed using some case studies where volcano eruption happened in proximity of an available weather radar:

— Grímsvötn eruption in 2004, analyzed together with the Icelandic Met Office (IMO) (for details, see Marzano et al., 2006b, 2010a);

— Augustine eruption in 2006, analyzed together with the USGS Alaska Volcano Observatory (for details, see Marzano et al., 2008, 2010b).

1. **ICELAND**. Grímsvötn is one of the most active volcanoes in Iceland, with a ~62 km2 caldera covered by 150- to 250-m-thick ice. Its highest peak, Grímsfjall, on the southern caldera rim, reaches an elevation of 1722 m. Volcanic eruptions, numbering several per century, are phreato-magmatic because of the ice cover, and they usually persist for days to weeks. Geothermal activity continuously melts the overlying ice, and meltwater accumulates in a sub-glacial lake within the caldera until the surrounding ice is breached. Volcanic eruptions in Grímsvötn often coincide with jökulhlaups. On the morning of Nov. 1 a jökulhlaup tremor was observed on the seismic records at the Grímsfjall station. The Grímsvötn eruption started in the evening of Nov. 1, 2004 and was observed by a C-band weather radar located in Keflavik, Iceland [20]. The first plume detected by the Keflavik radar was at 23:05 UTC (Universal Time Coordinate) on Nov. 1, 2004. Lightning over Grímsvötn, which accompanied the rising plume, was eventually seen at about 03:00 UTC, but darkness and weather conditions prevented visual observation of the eruption site. The eruption on night of Nov. 2 was followed by frequent plumes and the last one, detected by the weather radar, was at 08:30 UTC on Nov. 3. After this time, the plume was too low to be detected by the radar (reaching 6 km height or less). Radar volume scans were continuously acquired and data have been made available from 23:00 on Nov. 1, 2004 till 06:00 UTC on Nov. 2, 2004 every half an hour. Reflectivity data were radially averaged to 2 km. in order to increase the measurement sensitivity (equal to about −5 dBZ around 260-km range). Considering the distance of about 260 km between the Keflavik radar and the Grímsvötn volcano, volcanic ash clouds can be detected at heights higher than about 6 km using the minimum elevation of 0.5°. This means that the volcanic eruption cloud cannot be detected between the Grímsvötn summit at 1725 m and 6000 m altitude. By comparing this range with the expected freezing level (around 1350 m) and considering the phreato-magmatic nature of Grímsvötn eruptions, we may expect the formation of ice particles and combination processes within the ash plume such as ice nucleation around ash nuclei.

2. **ALASKA**. The Augustine volcano is 1260-m high (4134 ft) and is a conically-shaped island stratovolcano located in southern Cook Inlet, about 290 km (180 mi) southwest of Anchorage, Alaska. The Augustine volcano is the most active volcano in the Cook Inlet region with five significant eruptions (1883, 1935, 1963-64, 1976, 1986) prior to 2006. These eruptions were primarily explosive events that produced volcanic ash clouds at their onset, followed by the emplacement of summit lava domes or flows. The explosive phase of the 2006 eruption consisted of thirteen discrete Vulcanian explosions from January 11 to 28, with seismic durations that ranged from one to eleven minutes. These violent explosive events are characterized by the ballistic ejection of volcanic blocks and bombs, the emission of volcanic ash, and were accompanied by atmospheric pressure wave. Cloud heights during this phase varied from 7.5 to 14 km above sea level. The character of the eruption changed to a more continuous ash emission phase from January 28 to February 2 that produced ash plumes at lower altitudes (below

4 km above sea level). The ability of the NEXRAD radar to provide near real-time updates on the position and altitude of volcanic ash clouds was vital in providing timely and accurate forecasts and warnings. One of the most significant contributions made by the radar data was in short term aviation forecasting. Radar cross sections were routinely used for diagnosing the vertical disposition of ash clouds during each event. These observations, in tandem with pilot reports, were used to ascertain the vertical extent of the ash clouds and issue timely advisories to the aviation community. The ability to track the volcanic ash in the short-term was also vital to issuing timely and location-specific volcanic ashfall advisories. The ability to monitor the movement of the volcanic ash cloud on a minute by minute basis was essential given the close proximity of Augustine to settlements around the Cook Inlet region. In addition, marine weather statements were issued, alerting mariners to the potential hazards posed by the volcanic ash. The VARR retrieval procedure was applied to WSR-88D S-band radar data available during the eruption of the Augustine volcano on 13 January 2006. The evolution of the Augustine Vulcanian eruption is discussed in terms of radar measurements and examples of the achievable retrieval algorithm products are presented and discussed.

Preliminary conclusions

The possibility of monitoring 24 hours a day, in all weather conditions, at a fairly high spatial resolution and every few minutes after the eruption is the major advantage of using ground-based microwave radar systems. The latter can be crucial systems to monitor the volcanic eruption from its eruption early-stage near the volcano vent, dominated by lapilli and blocks thephra, to ash-dispersion stage up to few hundreds of kilometers, dominated by transport and evolution of coarse and fine ash particles. Of course, the sensitivity of the ground-based radar measurements will decrease as the ash cloud will be farther so that for distances greater than about 50 kilometers fine ash might become “invisible” to the radar; but, in this respect, radar observations can be complementary to satellite, lidar and aircraft observations. Moreover, radar-based products such as real-time erupted volcanic ash concentration, height, mass and volume can be used to initialize dispersion model inputs.

Due to logistics and space-time variability of the volcanic eruptions, a suggested optimal radar system to detect ash cloud could be a portable X-band weather Doppler polarimetric radar. This radar system may satisfy technological, economical and new scientific requirements to detect ash cloud. The siting of the observation system which is problematic tradeoff for a fixed radar system (as the volcano itself may cause a beam obstruction and the plume may advect in unknown directions), can be easily solved by resorting to portable systems.

An overall algorithm for X-band radar polarimetric retrieval of volcanic ash clouds from measured dual-polarization reflectivity can be devised extending the VARR approach. It can be based on four cascade steps: i) monitoring of active volcano through a method based on analysis of reflectivity radar data time series associated with in-situ information and satellite-derived products; ii) tracking of ash plume based on a pattern matching approach applied on radar images; iii) classification of ash plume through a method based on the vectorial Bayesian theory; iv) retrieval of ash amount and fall rate from the measured reflectivity through parametric models. The expected accuracy of the VARR algorithm estimates can be evaluated using a synthetic data set. In order to quantitatively evaluate the ash detectability by weather radars, a sensitivity analysis can be

preliminarily performed by simulating a synthetic ash clouds and varying ash concentration and size as function of the range.

The major recommendation of this document is that dual polarization ground-based weather radars can be successfully used for volcanic ash cloud dynamical monitoring and quantitative retrieval of ash category, concentration and fall rate. Of course, the expected accuracy is conditioned by the microphysical assumptions, chosen to constrain the inverse problem, even though the Bayesian retrieval approach can easily ingest the knowledge of these uncertainties within the VARR scheme. It is intuitive and has been here demonstrated that the radar detectability of moderate-to-low concentration fine ash is improved if, for the same configuration, the available peak power is higher, the radial resolution is larger and the observation distance is shorter.

Further work is needed to assess the VARR potential using experimental campaign data. Future investigations should be devoted to the analysis of the impact of ash aggregates on microwave radar reflectivity and on the validation of radar estimates of ash amount with ground measurements where available. The last task is not an easy one as the ash fall is dominated by wind advection and by several complicate microphysical processes. This means that what retrieved within an ash cloud may be not representative of what collected at ground in a given area. Spatial integration of ground-collected and radar-retrieved ash amounts may be considered to carry out a meaningful comparison.

References

Marzano F.S., E. Picciotti, G. Ferrauto, G. Vulpiani, and W. I. Rose, "Volcanic ash remote sensing by ground-based microwave weather radar," in Proc. General Assem. EGU, Vienna, Austria, Apr. 25–29, 2005, pp. 212–215. Wien (A).

Marzano F.S., S. Barbieri, G. Vulpiani and W.I. Rose, "Volcanic cloud retrieval by ground-based microwave weather radar", IEEE Trans. Geosci. Rem. Sens., vol. 44, n.11, pp. 3235-3246, 2006a.

Marzano F.S., G. Vulpiani, and W.I. Rose, "Microphysical Characterization of Microwave Radar Reflectivity Due to Volcanic Ash Clouds", IEEE Trans. Geosci. and Rem. Sens., vol. 44, pp. 313-327, 2006b.

Marzano F.S., S. Marchiotto, S. Barbieri, D. Schneider, C. Textor and G. Giuliani, "Ground-based radar remote sensing of explosive volcanic ash eruptions: numerical models and quantitative applications", Proc. of USE of Remote Sensing Techniques (USEReST) for Monitoring Volcanoes and Seismogenic Areas, Naples, Italy, November 11-14, 2008.

Marzano F.S., S. Barbieri, E. Picciotti and S. Karlsdóttir, "Monitoring sub-glacial volcanic eruption using C-band radar imagery", IEEE Trans. Geosci. Rem. Sensing, vol. 58, n. 1, pp. 403-414, 2010.

Marzano F.S., S. Marchiotto, S. Barbieri, C. Textor and D. Schneider, "Model-based Weather Radar Remote Sensing of Explosive Volcanic Ash Eruption", IEEE Trans. Geosci. Rem. Sensing, in press, 2010b.

Annex 2a - Description of Some European Ash Transport Models

A. Stohl[1], F. Prata[1], H. Elbern[2] , S. Scollo[3] and S. Varghese[4]

[1] Norwegian Institute for Air Research, [2]University of Cologne, [3]Istituto Nazionale di Geofisica e Vulcanologia, [4]National University of Ireland

London VAAC model

The Met Office's capability to predict the transport and spread of pollution is delivered by the NAME (Numerical Atmospheric-dispersion Modelling Environment) computer model. The model began development following the Chernobyl accident in 1986 and since that time it has been used to model a wide range of atmospheric dispersion events, including previous volcanic eruptions and the Buncefield explosion in 2005. In addition to its role as emergency response guidance tool the model is used for routine air quality forecasting and meteorological research activities. NAME provides a flexible modelling environment able to predict dispersion over distances ranging from a few kilometres to the whole globe and for time periods from minutes upwards.

NAME is a 'Lagrangian' particle model which calculates the dispersion of pollutants by tracking model 'particles' through the modelled atmosphere (Jones et al. 2007). The process is initiated by the emission of model particles into the atmosphere. NAME has the flexibility to specify point or extended sources at any location in the atmosphere, together with relevant source parameters such as the mass emission rate, emission velocity and temperature. Once emitted, particles move in a manner determined by the meteorology, which is input separately to the model. NAME uses meteorological parameters derived from the main Met Office weather forecast model MetUM (the Met Office Unified Model). The most important parameters are the wind speed and direction, which vary in all three dimensions and in time. However other meteorological parameters are used by NAME, such as the vertical temperature profile (which determines the atmospheric stability with respect to vertical motion) and the height of the atmospheric boundary layer (which is important for predicting the short-term spread of pollutants emitted at the surface and sedimentation). NAME includes a model for deep convective transport. In addition to the movement of particles by the prescribed meteorological winds the particle motion also has a random component to represent the effects of atmospheric turbulence.

Once emitted and being transported by atmospheric motions, pollutants in NAME simulations can also be removed from the model atmosphere by several processes; i) fall out due to gravity, ii) impaction with the surface, iii) washout where the pollutant is 'swept out' by falling precipitation and iv) rainout where the pollutant is absorbed directly into cloud droplets as they form. In addition each model 'particle' can have its own characteristics, for example, particles can represent different compounds or chemicals and particles can have real and different particulate sizes. NAME also includes a chemistry scheme for common atmospheric chemical components.

Toulouse VAAC model

MOCAGE-accident is a specific version of the MOCAGE (Modèle de Chimie Atmosphérique à Grande Echelle) three-dimensional chemistry and transport model developed by Météo-France tuned for the transport and diffusion of

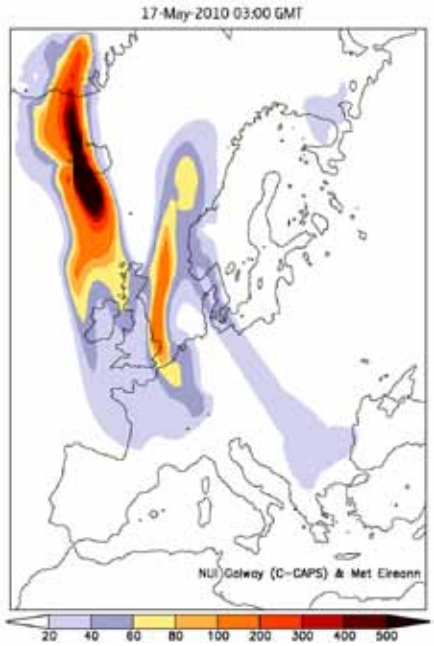

Fig. 2a1. REMOTE model forecast of volcanic ash column burden distribution (mg/m2) for 17 May, 2010, 03:00 GMT simulated with available information of Eyjafjöll volcano source parameters.

accidental release from the regional to the global scale. Only dynamical and physical processes are taken into account, excluding chemistry. MOCAGE-accident runs in off-line mode, using Météo-France ARPEGE or ECMWF/IFS operational NWP products as dynamical forcings. Meteorological forcings (hydrostatic winds, temperature, humidity and pressure) feed the advection scheme, as well as the physical parameterizations. They are considered every 6 hours, and are linearly interpolated to yield hourly values, consistent with the time-step for advection; smaller time-steps are used for physical processes, but the meteorological variables are kept constant over each hour.

MOCAGE-accident can be run for an emission taking place everywhere over the globe. In the operational configuration, it has a 0.5° horizontal resolution and 47 hybrid (σ,P) levels from the surface up to 5 hPa, with approximately 7 levels in the planetary boundary layer, 20 in the free troposphere and 20 in the stratosphere. In this way, the model can consider emissions in the first meters above the surface as well as over thousands kilometres up to the stratosphere. When the pollutant is volcanic ash, sedimentation of the particles is taken into account in addition to processes represented for tracers. MOCAGE-accident can also be run in "inverse" mode in order to provide information on the origin of an air-mass arriving at a given point in space and time.

Other European plume models

Various European research groups are capable of running volcanic ash plume simulations, sometimes even in an operational fashion. Within the GMES framework, the MACC and PASODOBLE projects run global and regional models. These models were designed for monitoring atmospheric composition in general, but can be used for specific issues like volcanic eruptions as well. The MACC systems are also capable to use data assimilation to constrain the model forecasts. The global MACC model is based on the ECMWF IFS system which uses semi-Lagrangian transport on a reduced Gaussian grid. As an instant action shortly after the eruption the MACC global model simulated the plume by a total column tracer proxy. The European continental scale model EURAD-IM (EURopean Air pollution Dispersion-Inverse Model), which features full gas phase and aerosol particle dynamics and chemistry, and displayed ash plume simulations for over a month in 15 km horizontal resolution . This model proved to be easily adapted to volcanic ash and gas eruption modelling, including full gas phase chemistry, aqueous phase chemistry, as well as aerosol dynamics and chemical formation,dry and wet removal, and cloud interaction. For variational inverse modelling, adjoint components of principal process modules are available and applied for source strengths inversion with air quality conditions (Elbern et al., 2007). It is clearly desirable, for ash quantification, which fraction of remotely sensed aerosol is due to sulfates or the, non ash component. This however, requires an observing network, which is usually unavailable apart from well compiled measurement missions. Coupling with a meteorological model (MM5 and WRF, consistent vertical winds are available. A remarkably well coincidence with modelled and LIDAR observed height levels could be demonstrated. After in situ observations were available from GAW Zugspitze observatory, quantitative simulations could be provided (Figure 7).

FLEXPART is a Lagrangian particle transport model (LPDM), similar to the NAME model used at the London VAAC. FLEXPART calculates the trajectories of tracer particles using the mean winds interpolated from the analysis fields plus random motions representing turbulence (Stohl et al., 2005). Unlike most other LPDMs, FLEXPART also has a parameterization for deep convective transport. FLEXPART also treats wet and dry deposition as well as gravitational settling and can simulate transport of particles of different sizes. FLEXPART was validated with data from continental-scale tracer experiments (Stohl et al., 1998) and has been used in a large number of studies on long-range

Table 2a1. Some models used for volcanic ash transport and dispersion forecasts.

Model name	Institution	Type of model	Reference
Operational			
NAME	London VAAC	Lagrangian	Ryall and Marion (1998)
HYSPLIT	Washington VAAC + Darwin VAAC + many others	Lagrangian	Draxler and Hess (1998)
PUFF	Alaska Volcano Observatory	Lagrangian	Searcy et al. (1998), Webley et al. (2009)
MLDP0	Montreal VAAC	Lagrangian	D'Amours (2010)
MOCAGE	Toulouse VAAC	Semi-Lagrangian	Josse et al. (2004)
FALL3D	Istituto Nazionale di Geofisica e Vulcanologia, Osservatorio Vesuviano	Eulerian	Folch et al. (2009)
Some R&D models as discussed during the workshop			
FLEXPART	NILU + many others	Lagrangian	Stohl et al. (1998), Stohl et al. (2005)
EURAD-IM	University Cologne	Eulerian	Elbern et al., (2007)
REMOTE	National University of Ireland	Smolarkiewicz Scheme	Langmann et al., (2008)

atmospheric transport. The reference version of FLEXPART can ingest meteorological data from either the European Centre for Medium-Range Weather Forecasts or from the National Center for Environmental Prediction's (NCEP) Global Forecast System (GFS) model. There are also many other versions using other meteorological data (e.g. from MM5, WRF, COSMO, etc.). FLEXPART is used by many dozen research groups worldwide and is used operationally for emergency preparedness in Austria and fur nuclear explosion source attribution at CTBTO. Simulations of volcanic plume dispersions are described in Prata et al. (2007), Wang et al. (2008), Eckhardt et al. (2008), Bitar et al. (2010), Hoffmann et al. (2010) and Kristiansen et al. (2010).

Another model used for volcanic ash forecasts is the regional scale air-quality/climate model REMOTE (Langmann, 2000; Langmann et al., 2008) at the National University of Ireland, Galway. This hydrostatic three-dimensional model uses the ECMWF meteorology forecast data for boundary forcing every 6 hours. REMOTE is coupled with the gas-phase chemistry (RADM2) and aerosol dynamics (M7) modules and has advanced treatment for sedimentation, dry deposition and wet deposition. The input parameters for volcanic ash modelling includes plume height, emission rate, vertical distribution of emission, density of ash, distribution in the different size modes and the mode median radius of the particles. The particles are treated as insoluble and are introduced in a log-normal distribution into the different size modes. Figure 2a1 shows a typical forecast of volcanic ash concentration from the REMOTE model.

Various other plume models exist in Europe (e.g. TM4, SILAM) and, while not described in this working paper directly, should be included in collaborative efforts on model improvements.

In Volcanology, there are several tephra dispersal models which have been validated comparing model outputs with field data of tephra deposits. Examples are:

— HAZMAP applied to the vulcanian explosions and dome-collapses from the 1995–1999 eruption of Soufrière Hill Volcano in Montserrat (Bonadonna et al., 2002), to the 79 AD Plinian eruption of the Vesuvius (Pfeiffer et al., 2005) and 21-24 July 2001 Etna eruption (Scollo et al., 2007).

— TEPHRA (Bonadonna et al., 2005) validated on data of the 17 June 1996 andesitic sub-Plinian eruption of Ruapehu, New Zealand.

— FALL3D (Costa et al., 2006) and VOLCALPUFF (Barsotti et al., 2008) validated using field data of 21-24 July 2001 Etna eruption.

— PUFF (Searcy et al., 1998) validated comparing model results with the tephra deposit the 1980 eruption of Mount St. Helens (Fero et al., 2008).

ANNEX 2b - Physical Volcanology Contribution to the Document on the Ash Crisis – Eyjafjöll Eruption – Iceland 2010.

By S. Tait – French Volcanologic and Seismologic Observatories

Introduction

Explosive volcanic eruptions generate ash-laden jets that emerge from the vent at speeds typically on the order of 100 to several hundred m.s-1. The ash is generated by fragmentation: the magma is transformed into a gas jet bearing particles with a range of characteristic sizes from on the order of 10 cm down to the order of a micron (see below). The small size of the fragments ensures highly efficient transfer of heat from the hot fragments to the air that is entrained into the jet by vigorous turbulent mixing. It is the heated gas that gives the jet sufficient buoyancy to rise in the stratified atmosphere until it reaches a maximum height and then spreads out at its level of neutral buoyancy. The difference between the maximum height and the level of neutral buoyancy depends on the momentum the plume possesses when it first attains the neutral buoyancy level. The horizontal part of the flow is a gravity current, known as the umbrella region.

The height reached in the atmosphere by a plume is fundamentally related to the flux of material that is ejected at the vent, e.g. the thermal power liberated at the source. At the low end, source mass fluxes can be on the order of 105 kg.s-1 (which was roughly the case for the Eyjafjöll plume) but at the high end can be 109 kg.s-1), or perhaps even higher, a huge variation. Whereas a relatively weak plume can plausibly be treated as a source of particles that is passive from the point of view of the atmospheric circulation, this will not be the case for a very strong plume.

Maximum plume height, particle loading, particle size distribution are quantities that are not always easy to measure but can be understood in the framework of physical models which fit the existing data quite well. Below we summarize salient features of our current knowledge of explosive volcanism and the processes by which volcanic ash is produced and injected into the atmosphere. More details or a library of relevant calculations and figures could be provided if necessary. The idea is to give a general framework in which the specific case of the Eyjafjöll can be situated.

Fragmentation and particle size distribution

Fragmentation begins in the volcanic conduit through which magma rises to the surface and consequently « sees » a continuously decreasing pressure. This leads first to the magma becoming saturated with respect to a volatile phase and then to a progressively greater proportion these volatiles exsolving from the magma to produce bubbles. Although the mass fraction of volatiles in magma is small (typically a few weight percent), the expansion of the volatile phase under the influence of decompression is such that the volume fraction becomes very large near to the vent and the bubbles connect and disrupts the magma into fragments. This process proceeds with more and more particle collisions producing a larger and larger fraction of small particles. The lower limit of particle size is determined typically by the smallest bubbles which by observation are on the order of a micron. Secondary fragmentation processes such as explosive interaction with aquifers or surface water and ice (as in the case of Eyjafjöll) can further enhance the production of fine particles.

The coarsest particles tend to be deposited close to the vent and the finer particles carried away by the plume and then atmospheric currents to large distances so that reconstruction of the total grain size distribution is an arduous task. For a few tens of eruption deposits enough data exists to attempt a reconstruction of the generic features. It has been shown that the grain size populations can be described by a power law in the sense defined below.

Volcanologists adopted a convention from sedimentology and use so-called f units which is based on sieve sizes

$$\varphi = -\frac{\log d}{\log 2}$$

where d is the maximum length of a fragment in mm. In other words the particle diameter is 2-f in mm. The total mass of particles in the deposit in a given sieve size is found by integration based on observations made at given locations and a simple mathematical description of how the deposit thickness declines with distance from the source and the shape of contours of iso-thickness (so-called isopachs). It is found that a good mathematical fit to the data is obtained using a power law description. If N (R>r) is the number of fragments greater than size r, then

$$N = \lambda . r^{-D}$$

where l is a normalization constant. If the number of fragments in each sieve class f is called D(f), then the data can be described by:

$$\ln_2(\Delta(\phi)) = \ln_2(N_o) - D\varphi$$

where No is a normalization constant. Figure 2b1 shows examples of grain size distributions reconstructed from two deposits – one is from the eruption of 1875 of the Icelandic volcano Askja, and the other is the Hachinohe deposit from northern Honshu in Japan - showing D values of 3 and 3.5 respectively. Laboratory experiments show that primary breakup leads to D values of 2.5 +/- 0.1 and that subsequent repeated or secondary fragmentation processes act to increase D. The range of D values found from deposits that sedimented from eruption columns is typically 3.0 to 3.9. There is a tendency for the smallest particles to be transported away in the atmosphere and not to be preserved in the deposit, but the data that exist are consistent with this approach and it is reasonable to assume that a power law is valid down to the smallest sizes. The high values of D from volcanic deposits indicate that fragmentation is a progressive process. The strong interaction between ice and magma in the Eyjafjöll eruption suggests that the expected D value would be relatively high and the proportion of small particle sizes relatively large.

Fig. 2b1. Two examples of power law size distributions from volcanic eruption deposits.

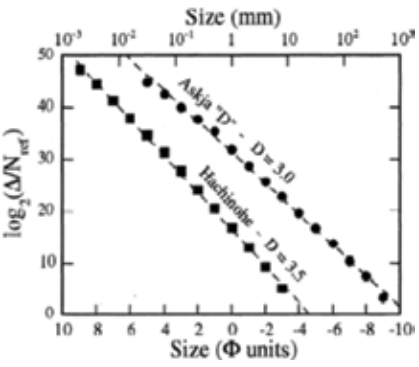

Plume dynamics

Volcanic plumes are driven by the heat transferred from the small particles to atmospheric air that is entrained into the eruption jet by vigorous turbulent mixing. In the case of strong fragmentation and a vigorous eruption, it is reasonable to assume that all of the heat from the magma goes to feeding the plume, and the theory of turbulent jets and plumes can be used to obtain a prediction of the behaviour in the atmosphere. Complications can arise in the exit conditions such as over-pressure that leads to shock waves, but experience has shown that after a relatively brief decompression phase just above the vent, it is reasonably accurate to assume that the plume is a narrow object,

in pressure equilibrium with the surrounding atmosphere, which allows important theoretical simplifications.

Three fundamental things affect the height that will be reached in the atmosphere and the concentration of ash present at the top of the plume. These are, the mass flux (Qo) at the source, the vertical profile of atmospheric density (S) above the source and the rate of entrainment by turbulent mixing. Although some direct numercial simulations have been carried out firstly in a 2D asymmetric geometry and more recently in 3D, the most efficient models are so-called « top hat » models in which it is assumed that, at any given height, the jet or plume has characteristic values of radius, vertical velocity and buoyancy (dependent on gas temperature and particle load). These three variables are calculated as a function of height until the vertical momentum drops to zero at the maximum height (Hmax). These models require an empirical entrainment coefficient (ae) which, in a first generation of models, was assumed to be a universal constant. In more recent work, validated by comparison with experimental results, it has been shown that the ae is a variable which depends notably on the buoyancy of the jet via the Richardson Number. This is important because the buoyancy of the jet is negative when it comes out of the vent, becomes positive because of all the entrained and heated air, then negative again between the neutral buoyancy level and the maximum height.

The fundamental dependence of the maximum height reached as a function of the above variables is:

$$H_o = (2.\alpha_e)^{-0.5} . F_o^{0.25} . S^{-0.75} \qquad \text{with} \qquad S = -\frac{g}{\rho_r} . \frac{d\rho_a}{dz}$$

ra and rr are the atmospheric and a reference density respectively and z is the vertical co-ordinate.

One cannot give one universal curve valid for all explosive volcanic eruptions because the atmospheric stratification varies between tropical and polar regions, because the entrainment coefficient varies according to the buoyancy evolution of the plume, and because the amount of volatiles exsolved from the magma varies from case to case. Nevertheless, the general behaviour is well described by the above relationship and calculations in specific cases give good results. Figure 2b2 shows curves relating the mass discharge at the source (Qo) to the maximum height for different atmospheric stratifications, for a generic situation of a given magma type. This graph shows that volcanic plumes can inject ash into the atmosphere at heights that can range from a few

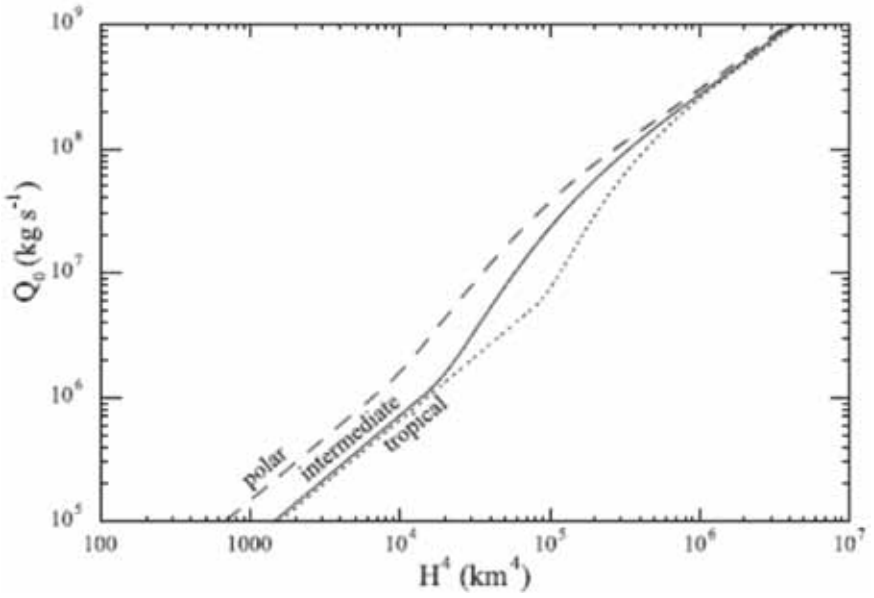

Fig. 2b2. REMOTE model forecast of volcanic ash column burden distribution (mg/m2) for 17th May, 2010, 03:00 GMT simulated with available information of Eyjafjöll volcano source parameters.

km to a few tens of km. and most importantly that the mass flux of particles and the height of injection are not independent. The mass flux of an explosive eruption determines the environmental impact of an eruption but it is notoriously hard to measure in real time because of the inherent danger of such events. Hence volcanologists typically use the above formalism to measure mass flux indirectly via observations of plume height. In eruptions of known duration and whose total output can be estimated after the fact, an average mass flux can be estimated.

The Eyjafjöll eruption showed two major complications with respect to this generic analysis, which is based on a strong plume in a quiescent atmosphere, namely that the plume was weak and hence strongly bent over by the wind, and secondly that mass flux at the vent was being partitioned at the source: some material dropped back quickly to feed a lava flow on the ground, whereas the rest rose to feed the plume. This partitioning is not uncommon in relatively weak eruptions. It is also more common when the magma composition is basaltic rather than silicic, because the former have less volatiles to exsolve and fragmentation is hence less efficient. Unless good constraints are available from observations at the source to roughly quantify this mass partitioning, it becomes another source of uncertainty. Some idea of the potential quantitative impact of these complications is given in the paragraph below which discusses the ash loading in the umbrella cloud.

Ash loading and umbrella cloud

If the plume is very strong and effectively maintains in suspension the great majority of the ash particles, the ash loading at the top of the plume and hence in the umbrella cloud as it starts to spread can be calculated from the model summarized above. The buoyancy of the plume depends fundamentally on two factors, the temperature of the gas and the particle load. Horizontal spreading occurs when the plume reaches its level of neutral buoyancy in the atmosphere. The temperature of the gas is the dominant factor because this is sensitive to the mass (hence heat) flux at the vent. The calculated ash load is shown in figure 2b3a (for a given magma type, volatile content and exit velocity) as a function of total mass flux, and in figure 2b3b of the height reached by the plume. Ash load varies but weakly. The typical order of magnitude for the ash load in the umbrella cloud is 1000 mg.m-3. These graphs also show the results of some more preliminary calculations in which different percentages of the

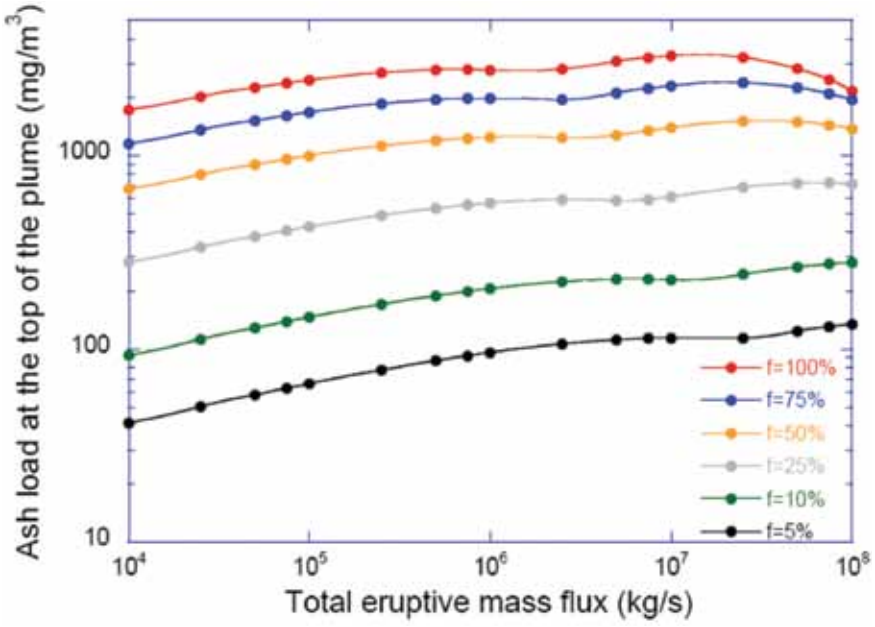

Fig. 2b3a. showing ash loading in the umbrella cloud near the source as a function of mass flux

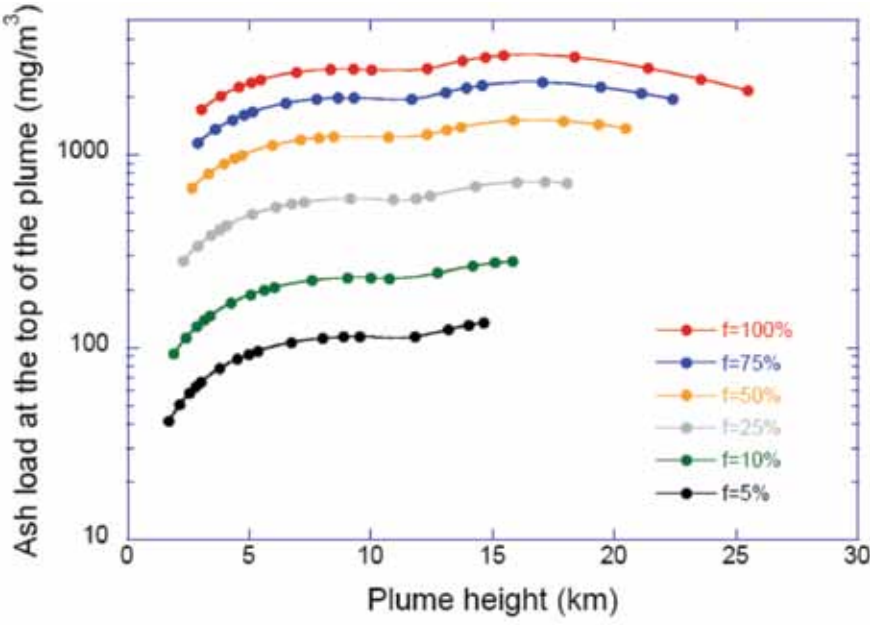

Fig. 2b3b. showing the same thing as a function of maximum height attained by the plume.

total mass flux are assumed to be injected into the plume. The reduction in ash loading does not vary exactly linearly with this percentage because all of the magmatic gas is always assumed to be injected into the plume, and the gas plays a dominant dynamic role. Ash loading drops as the fraction of the total mass flux injected into the plume decreases. Temporal variability in the height of the Eyjafjöll eruption plume may have been due to variations in the mass partitioning at the source, and one would expect that ash loading also varied. These calculations assuming mass partitioning give a preliminary indication of the order of magnitude we should expect and could be refined as necessary.

Conclusion

The main message is that relatively robust physical models of eruption columns exist and predict the heights reached in the atmosphere by eruption columns as a function of mass flux at the source. Because in practice, the latter has only been measured accurately for a few test cases of recent eruptions, in practice; volcanologists more commonly use column height to estimate the mass flux. Height and mass flux are not independent, but are intrinsically related by the plume dynamics. For strong plumes, the ash loading at the top of the column is also not independent, and the order of magnitude can be estimated within the model framework. For weak eruptions such as that of Eyjafjöll, the effect of crosswind and mass partitioning at the source between a lava flow and the plume introduce significant complications. The details of the particle size distribution are harder to know because these depend on the intensity of the fragmentation process and how it proceeds. Nevertheless a power law distribution for the particle sizes gives a good first order description. Secondary fragmentation processes such as magma-water or magma-ice interaction can significantly shift the size distribution to smaller values, and at present this is difficult to quantify.

The list of references includes some in which recent refinements of eruption models have been introduced which were used in the above discussion. The list also includes some older but more comprehensive reviews of eruption models, and also the pioneering paper by Morton Taylor and Turner (1956) on rise of a buoyant plume in a stratified environment.

References

Andronico, D., Scollo, S., Cristaldi, A., Caruso, S., 2008. The 2002–03 Etna explosive activity: tephra dispersal and features of the deposit. J. Geophys. Res. doi:10.1029/ 2007JB005126.

Barsotti, S., A. Neri, J. S. Scire, 2008. The VOL-CALPUFF model for atmospheric ash dispersal: 1. Approach and physical formulation, J. Geophys. Res., 113, B03208, doi:10.1029/2006JB004623.

Bonadonna, C., Macedonio, G., Sparks, R.S.J., 2002. Numerical modelling of tephra fallout associated with dome collapses and Vulcanian explosions: application to hazard assessment on Montserrat. In: Druitt, T.H., Kokelaar, B.P. (Eds.), The Eruption of Soufrière Hills Volcano, Montserrat, from 1995 to 1999. Memoir. Geological Society, London, pp. 517–537.

Bonadonna, C., Phillips, J.C., Houghton, B.F., 2005. Modeling tephra sedimentation from a Ruapehu weak plume eruption. J. Geophys. Res. 110, B08209. doi:10.1029/2004JB003515.

Cioni, R., Longo, A., Macedonio, G., Santacroce, R., Sbrana, A., Sulpizio, R., Andronico, D., 2003. Assessing pyroclastic fall hazard through field data and numerical simulations: Example from Vesuvio, J. Geophys. Res., 108(B2), 2063, doi:10.1029/2001JB000642.

Costa, A., Macedonio, G., Folch, A., 2006. A three dimensional Eulerian model for transport and deposition of volcanic ashes. Earth Planet. Sci. Lett. 241, 634–647.

Costa, A., Folch, A., Macedonio, G., 2010. A Model for Wet Aggregation of Ash Particles in Volcanic Plumes and Clouds: I. Theoretical Formulation, J. Geophys. Res., doi:10.1029/2009JB007175, in press.

Dubosclard, G., Donnadieud, F., Allard, P., Cordesses, R., Hervier, C., Coltelli, M., Privitera, E., Kornprobst, J., 2004. Doppler radar sounding of volcanic eruption dynamics at
Mount Etna. Bull. Volcanol. 56, 398–411.

Fero, J., Carey, S.N., Merrill, J.T., 2008. Simulation of the 1980 eruption of Mount St. Helens using the ash-tracking model PUFF. J. Volcanol. Geotherm. Res. 175 (3), 355–366.

D'Amours, R., A. Malo, R. Servranckx, D. Bensimon, S. Trudel, and J.-P. Gauthier-Bilodeau (2010): Application of the atmospheric Lagrangian particle dispersion model MLDP0 to the 2008 eruptions of Okmok and Kasatochi volcanoes. J. Geophys. Res., in press.

Draxler RR, Hess GD. 1998. An overview of the HYSPLIT-4 modelling system for trajectories, dispersion and deposition. Australian Meteorological Magazine 47: 295–308.

Folch, A., A. Costa, and G. Macedonio (2009): FALL3D: A computational model for transport and deposition of volcanic ash. Computers and Geosciences 35, 1334-1342.

Josse, B., Simon, P. and Peuch, V.-H. 2004. Rn-222 global simulations with the multiscale CTM MOCAGE. Tellus 56B, 339–356.

Ryall DB, Maryon RH. 1998. Validation of the UK Met. Office's NAME model against the ETEX dataset. Atmos. Environ. 32(24): 4265–4276.

Searcy C, Dean KG, Stringer W (1998) PUFF: a volcanic ash tracking and prediction model. J Volcanol Geotherm Res 80:1–16

Stohl, A., M. Hittenberger, and G. Wotawa (1998): Validation of the Lagrangian particle dispersion model FLEXPART against large scale tracer experiments. Atmos. Environ. 32, 4245-4264.

Stohl, A., C. Forster, A. Frank, P. Seibert, and G. Wotawa (2005): Technical Note : The Lagrangian particle dispersion model FLEXPART version 6.2. Atmos. Chem. Phys. 5, 2461-2474.

Webley, P. W, K. Dean, J. E. Bailey, J. Dehn and R. Peterson (2009): Automated forecasting of volcanic ash dispersion utilizing virtual globes,

Bitar, L., T. J. Duck, N. I. Kristiansen, A. Stohl, and S. Beauchamp (2010): LIDAR observations of Kasatochi volcano aerosols in the troposphere and stratosphere. J. Geophys. Res., in press.

Carazzo, G., E. Kaminski and S. Tait (2008). On the rise of turbulent plumes: quantitative effects of variable entrainment for submarine hydrothermal vents, terrestrial and extra-terrestrial explosive volcanism. Journal of Geophysical Research v.113, doi:10.1029/2007JB005458.

Eckhardt, S., A. J. Prata, P. Seibert, K. Stebel, and A. Stohl (2008): Estimation of the vertical profile of sulfur dioxide injection into the atmosphere by a volcanic eruption using satellite column measurements and inverse transport modeling. Atmos. Chem. Phys., 8, 3881-3897.

Elbern, H., A. Strunk, H. Schmidt, and O. Talagrand, Emission rate and chemical state estimation by 4-dimensional variational inversion, ACP, 3749-3769, 2007.

Hoffmann, A., C. Ritter, M. Stock, M. Maturilli, S. Eckhardt, A. Herber, and R. Neuber (2010), LIDAR measurements of the Kasatochi aerosol plume in August and September 2008 in Ny-Alesund, Spitsbergen, J. Geophys. Res., in press.

Hollingsworth, A., R.J. Engelen, C. Textor, A. Benedetti, O. Boucher, F. Chevallier, A. Dethof, H. Elbern, H. Eskes, J.Flemming, C. Granier, J.W. Kaiser, J. J. Morcrette, P. Rayner, V-.H Peuch, L. Rouil, M. Schultz, A. Simmons, and the GEMS consortium, 2008. Toward a monitoring and forecasting system for atmospheric composition. The GEMS Project. Bull. Amer. Meteor. Soc., 89, 1147 - 1164, doi:10.1175/2008BAMS2355.1

Jones A.R., Thomson D.J., Hort M. and Devenish B., 'The U.K. Met Office's next-generation atmospheric dispersion model, NAME III', in Borrego C. and Norman A.-L. (Eds) Air Pollution Modeling and its Application XVII (Proceedings of the 27th NATO/CCMS International Technical Meeting on Air Pollution Modelling and its Application), Springer, pp. 580-589, 2007.

Kristiansen, N. I., A. Stohl, A. J. Prata, A. Richter, S. Eckhardt, P. Seibert, A. Hoffmann, C. Ritter, L. Bitar, T. Duck, K. Stebel (2010): Remote sensing and inverse transport modeling of the Kasatochi eruption sulfur dioxide cloud. J. Geophys. Res., in print.

Langmann, B., 2000. Numerical modelling of regional scale transport and photochemistry directly together with meteorological processes, Atmos. Environ. 34, 3585-3598.

Langmann, B., Varghese, S., Marmer, E., Vignati, E., Wilson, J., Stier, P., O'Dowd, C.D., (2008). Aerosol distribution over Europe: A model evaluation study with detailed aerosol microphysics Atmos. Chem. Phys., 8, 1591-1607

Morton, B.R., Taylor, G.I. and Turner, J.S. (1956) Turbulent gravitational convection from maintained an instantaneous sources. Proc. Royal Soc. Lond. v.234, 1-23.

Oberhuber, J. M., M. Herzog, H. F. Graf and K. Schwanke (1998): Volcanic plume simulation on large scales, J. Volcanol. Geotherm. Res. 87, 29-53.

Prata, A. J., Carn, S. A., Stohl, A., and Kerkmann, J.: Long range transport and fate of a stratospheric volcanic cloud from Soufriere Hills volcano, Montserrat, Atmos. Chem. Phys., 7, 5093–5103, 2007.

Stohl, A., C. Forster, A. Frank, P. Seibert, and G. Wotawa (2005): Technical Note : The Lagrangian particle dispersion model FLEXPART version 6.2. Atmos. Chem. Phys. 5, 2461-2474.

Wang, X., A. Boselli, L. D'Avino, G. Pisani, N. Spinelli, A. Amodeo, A. Chaikovsky, M. Wiegner, S. Nickovic, A. Papayannis, M. R. Perrone, V. Rizi, L. Sauvage, and A. Stohl (2008): Volcanic dust characterization by EARLINET during Etna's eruptions in 2001-2002. Atmos. Environ. 42, 893-905.

Witham CS, Hort MC, Potts R, Servranckx R, Husson P, Bonnardot F (2007) Comparison of VAAC atmospheric dispersion models using the 1 November 2004 Grimsvötn eruption. Meteorol Appl 14:27–38

Annex 3a - Satellite Images

A.J. Prata - Norwegian Institute for Air Research

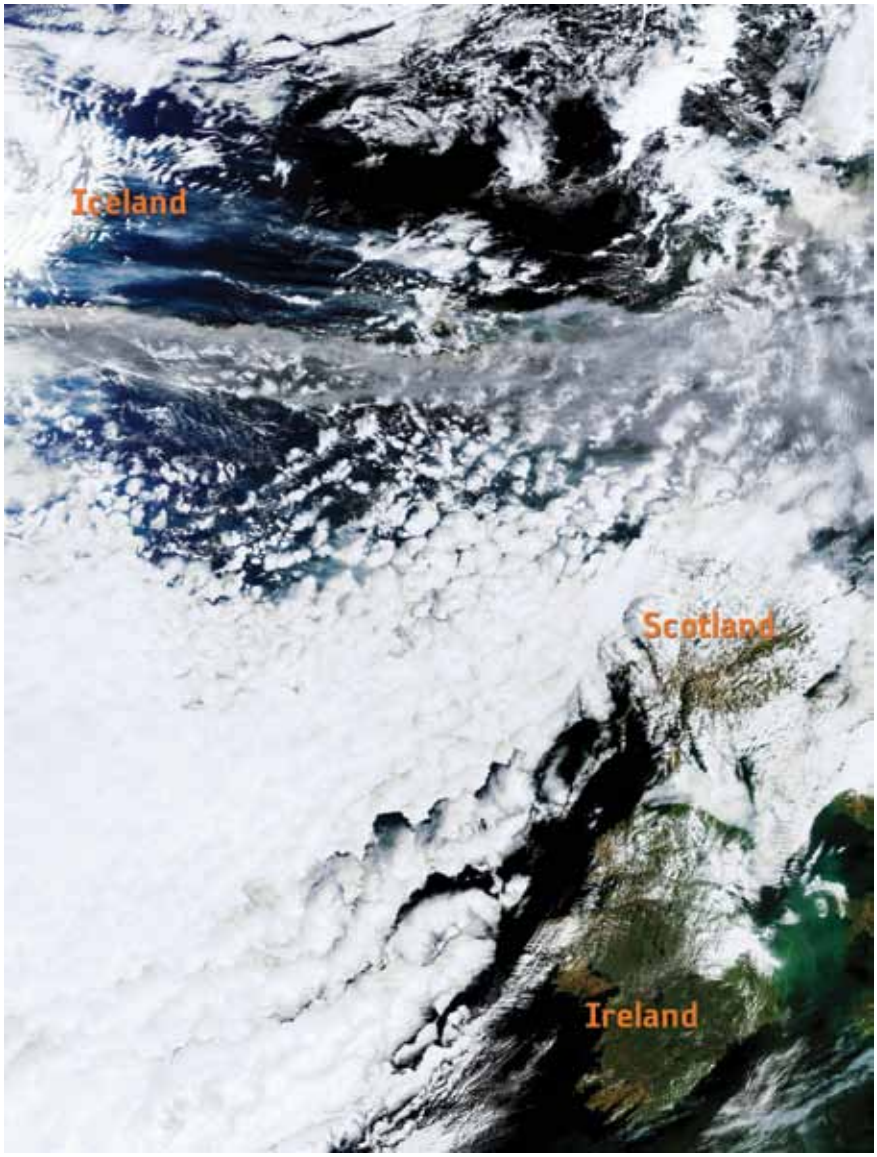

Fig. 3a1. MERIS true-colour image showing the volcanic cloud from Eyjafloll volcano. Images like this are excellent at identifying ash in the atmosphere when it is not obscured by clouds and only during daylight hours. Similar images were routinely used from MODIS (Terra/Aqua), AVHRR, GOSAT and SEVIRI. Apart from SEVIRI these instruments are in polar orbit and some have narrow swath widths making rapid and frequent identification of the plume difficult.

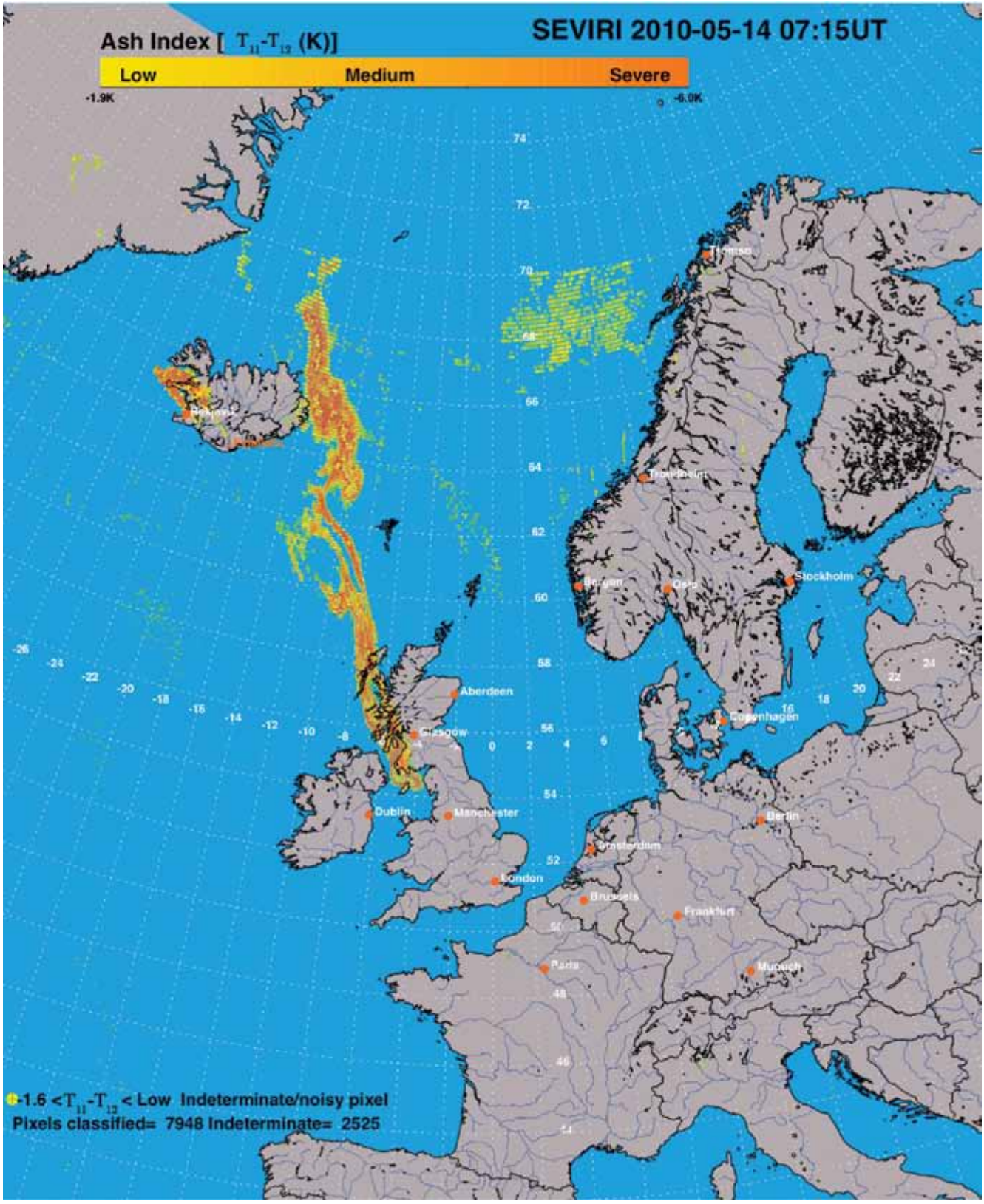

Fig. 3a2. Brightness temperature difference (BTD) image based on SEVIRI 11 and 12 μm infrared channels. Pixels coloured yellow – orange –red are idnetified as containing volcanic ash (not aerosol but ash). The detection limit (in this case DT=-1.9 K) can be adjusted, depending on the water vapour loading in the atmosphere.

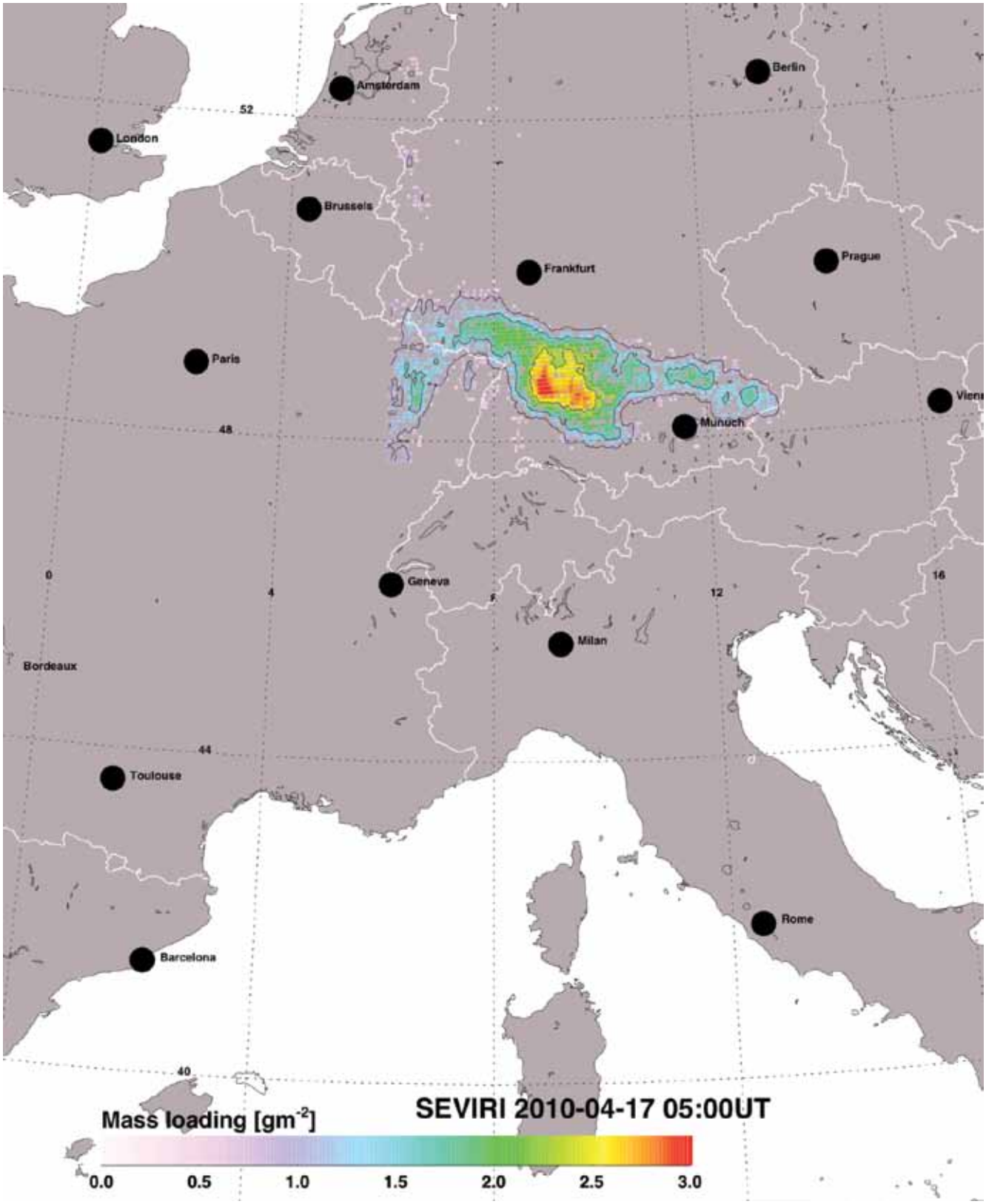

Fig. 3a3. Mass loading (gm-2) of ash retrieved from SEVIRI thermal infrared data for 17.04.2010 at 05:00UT, when simultaneous ground-based liadr observed the periphery of the ash cloud south of Munich.

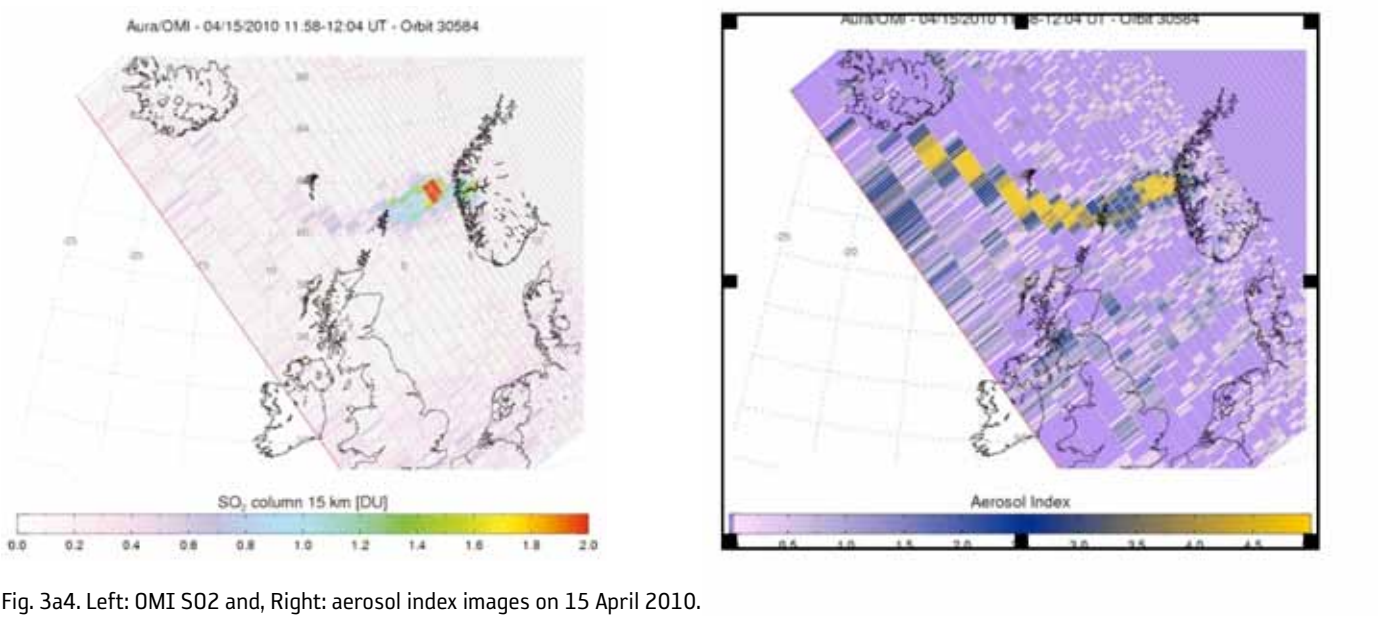

Fig. 3a4. Left: OMI SO2 and, Right: aerosol index images on 15 April 2010.

Annex 3b - The Reverse Absorption Algorithm

A.J. Prata - Norwegian Institute for Air Research

The basic principle of this algorithm for detecting ash uses the difference in absorption properties of silicate particles at two wavelengths in the thermal infrared. The two wavelengths used are 11 and 12 μm, but this is simply because these are the wavelengths generally available from several current (e.g. AVHRR, SEVIRI, MODIS) and planned (e.g. Sentinel/SLSTR) satellite instruments. The idea is to exploit the ratio of the extinction coefficients for ash at these two wavelengths as a means for discriminating ash from other atmsopheric particles. Since the extinction coefficients depend on refractive indices, particle sizes and shapes, it is also possible to perform a retrieval from the measurement space (11 and 12 μm brightness temperatures) to parameter space (infrared optical depth and effective particle size). We illustrate the technique here using highly simplified assumptions but noting that added complexity is simply a technical matter and offers marginal new insight into the principle.

Assume a gaseous-free atmospheric path with a homogenous single layer of ash cloud and monochromatic radiation. The for radiation at l1,

$$B_1 = \varepsilon_1 B_1(T_c) + (1-\varepsilon_1)B_1(T_s) \qquad (1)$$

Likewise for radiation at a second wavelength, l2:

$$B_2 = \varepsilon_2 B_2(T_c) + (1-\varepsilon_2)B_2(T_s) \qquad (2)$$

where Tc is the ash cloud temperature (assumed uniform) and Ts is the temperature of the enviornment behind the ash cloud (this could be the surface below, if viewing from a satellite).

Linearising these equations and after some manipultion it is possibe to derive the following:

$$\Delta T = \Delta T_c (X - X^{\beta}) \qquad (3)$$

where

It can be seen that the form of the relationship (3) depends on a few simple

$$\Delta T = T_1 - T_2$$

$$X = 1 - \frac{\Delta T_1}{\Delta T_c}$$

$$\Delta T_c = T_s - T_c$$

$$\Delta T_1 = T_s - T_1$$

$$\beta = \frac{k_1}{k_2}$$

$$\varepsilon_i = 1 - \exp(-k_i L)$$

parameters and in particular on the ratio of extinction coefficients at the two chosen wavelengths.

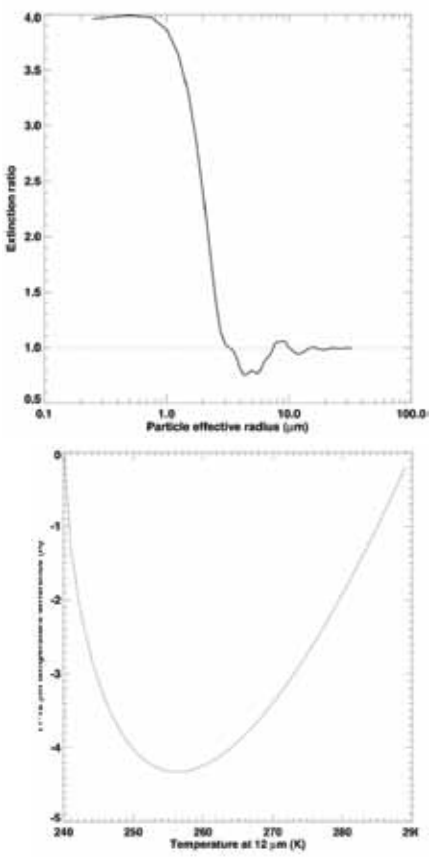

Fig. 3b1 Top panel:Extinction ratio (k1/k2) vs. effective particle radius for andesite particles. Bottom panel: 12μm brightness temperature vs 11-12 μm brightness temperature difference, showing the characteristic curve for ash particles (andesite) with effective particle radius of 5 μm and mass loading of 2 mgm-3. The temperature difference signal of –4K is easily detected using IR satellite data and demonstrates the great utility of these measurements for the ash hazard problem.

We note that when b<1, the curve of DT vs. T_2 is U-shaped, whereas if b>1 the curve is arch-shaped. Thus the shape of the distribution curve is a remarkably reliable indicator of the presence of ash in an image. The value of b depends on a number of factors, effective particle radius being of prime importance (see Figure 3b1).

In order to understand the sensitivity of this algorithm to silicate mass we will assume that the ash cloud consists of a monomodal size distribution with zero spread and particle radius of 5 μm. From A4 we see that k1= in this case.

The mass concentration (mgm-3) in a given pixel may be written,

$$M = \frac{4}{3}\rho r \frac{\tau_i}{k_i L} \qquad (4)$$

with r=2.6 x 106 gm-3; r=5 x 10-6 m; M=2 mgm-3; L= 1 km; k1=2.859 (k2=3.615); b=0.79; gives t1=0.30, and t2=0.38. We can also work backwards using these values in (1) and (2), and assuming values for Ts=290 K and Tc=240 K, results in the U-shaped curve shown in Figure 3b1 (right panel).

An example of an ash mass loading retrieval (i.e. M/L) is shown in Fig. A6.

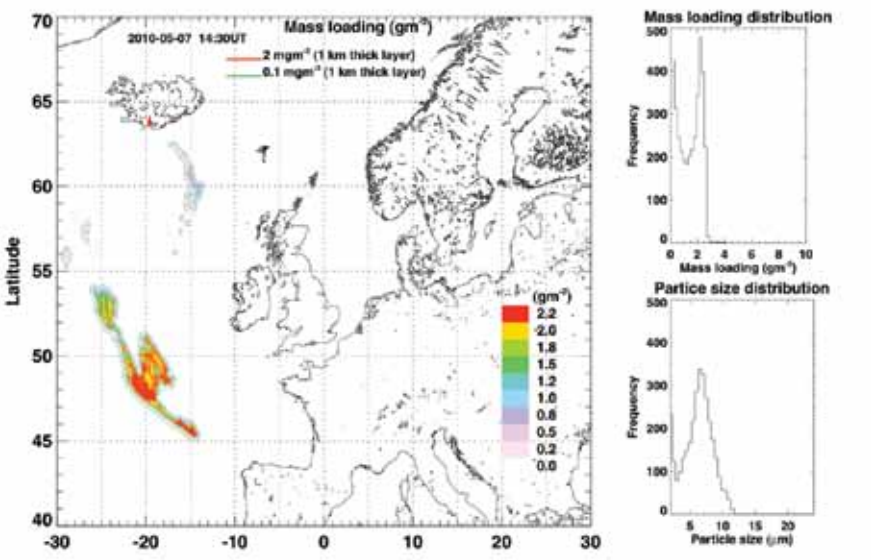

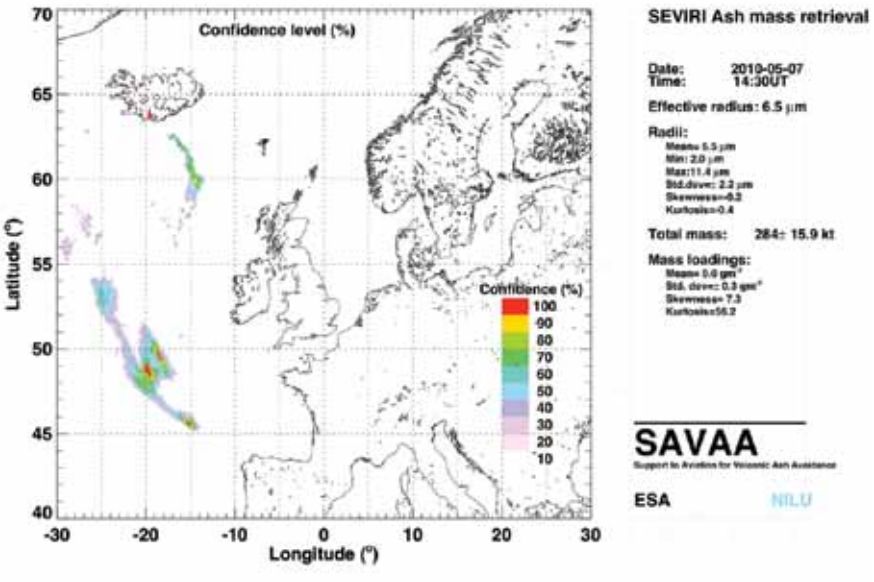

Fig. 3b2: Ash mass loadings (gm-2), confidence level (in %), mass distribution and effective particle size retrieval from SEVIRI infrared data.

Annex 3c - Future ESA/EUMETSAT satellite missions

T. Fehr[1] and R. Munro[2]

[1]ESA - European Space Agency, [2]EUMETSAT

Research Missions

EarthCARE

Objectives
The Earth Clouds, Aerosols and Radiation Explorer Mission (EarthCARE) has been selected as an Earth Explorer Core Mission in 2004 to cover primary research objectives set out in the ESA Living Planet Programme. Its primary objective is to contribute to the understanding of the earth radiation budget by providing global observations of vertical cloud and aerosol profiles.

Specific targets addressed by the mission with relevance for the determination of volcanic ash include the observation of the vertical profiles of natural and anthropogenic aerosols on a global scale, their radiative properties and interaction with clouds. In addition, EarthCARE will allow the observation of the vertical distributions of atmospheric liquid water and ice on a global scale, as well as the cloud distribution, cloud-precipitation interactions and the characteristics of vertical motions within clouds.

Instruments
The EarthCARE mission objectives will be addressed by the synergistic use of active and passive sensors. The instrument suite will consist of an ATmospheric LIDar (ATLID), a Cloud Profiling Radar (CPR), a Multi-Spectral Imager (MSI) and a BroadBand Radiometer (BBR). For the optimal exploitation of the data, the instruments footprints are carefully aligned (see Fig 3c1).

Atmospheric Lidar - ATLID
ATLID is a UV backscatter lidar at 355 nm emitting circular polarised pulses. It is equipped with a high spectral resolution receiver allowing the separation of the Rayleigh and Mie backscatter return. The receiver includes a cross-polar and a co-polar Mie channel, as well as a Rayleigh channel. The nominal horizontal sampling is 200 m with a vertical sampling of 100 m, and an altitude range covering -0.5 km to 40 km.

Cloud Profiling Radar - CPR
The CPR is a JAXA contribution to the EarthCARE mission. It is a high power millimetre-wave Doppler radar for the measurement of vertical profiles of clouds along the sub-satellite track. It emits microwave pulses at an operating frequency of 94 GHz, with a sensitivity of at least -35 dBZ at 20 km altitude. The altitude range covers -0.5 km to 20 km. The vertical resolution is 500 m with a sampling interval of 100 m. The Doppler accuracy is expected to be 1 m/s

Multi-Spectral Imager - MSI
The MSI is a nadir viewing push-broom imager with seven spectral channels at 670 nm, 865 nm, 1.65 µm, 2.21 µm ("solar" channels") and at 8.80µm, 10.80 µm, 12.00µm ("TIR channels"). It swath extends from -35 km to 115 km with respect to nadir with a sampling distance of 500 m.

Broadband Radiometer - BBR
The BBR measures the earth radiance a short wave channel between 0.2 µm and 4 µm, as well as in a long wave channel covering 4 µm to 50 µm. To cover the total radiance field, observations of the same area will be done in a forward-, nadir- and backward-looking view with a 10x10 km ground spot.

Orbit Parameters
EarthCARE will be operated in a sun synchronous orbit at a mean local solar time which will be fixed at a value between 13:45 and 14:00. The foreseen repeat cycle will be 25 days with a mean geodetic altitude of 408 km.

Products
EarthCARE will provide a broad range of products that can be retrieved from single sensors as well as through the exploitation of the synergy between the instruments. The list of EarthCARE Level 2 products is not consolidated; several product studies are on-going.

Potential products with relevance to the volcanic ash observations will include the Lidar backscatter, extinction and depolarisation ratio, target classification and aerosol layer descriptor, the imager aerosol optical thickness and Angstrom coefficient over oceans, the radar reflectivity, cloud mask, cloud particle type identification and vertical motion.

Foreseen synergetic products include target classifications, aerosol extinction coefficients, Aerosol spectral optical thickness, aerosol particle size, aerosol type and convective velocity.

The product list above is not exhaustive and not confirmed.

Currently only off-line processing of the EarthCARE products is foreseen. However, the requirements for a near real-time processing are under review.

Mission Status
The launch of the mission is currently foreseen in October 2014. The design lifetime of the EarthCARE mission 3+1 years.

ADM-AEOLUS

Objectives
The primary, long-term objective of the Atmospheric Dynamics Mission Aelous is to provide observations of global wind profiles along the line-of-sight direction. The data will be assimilated into numerical forecasting models leading to an improvement in objective analyses and hence in Numerical Weather Prediction. The retrieval of aerosol properties was not a priority.

Instrument
The ÆOLUS payload is the High Spectral Resolution Lidar ALADIN with one single wavelength in the UV at 355 nm HSRL with a Rayleigh and a Mie channel. There is no depolarization capability and there are no complementary instruments. It is optimised for wind measurements therefore the retrieval of spin-off products is limited. The vertical sampling of the atmospheric layers is adjustable from 0.25 km to 2 km thickness. The lidar operates in a burst mode allowing 50 km measurements every 200 km (see Figure 3c2).

Orbit Parameter
ADM-Aeolus is in a sun-synchronous orbit with 18:00 MLST at ascending node with a 7-day repeat cycle. The mean altitude is 408 km.

Products
Apart from the atmospheric dynamics products, a cloud/aerosol mask, optical depths, scattering ratios and backscatter-to-extinction rations are foreseen.

Mission Status
The launch of ADM-Aeolus is foreseen in 2012. The mission design lifetime is 3 years, plus 3 months commissioning phase.

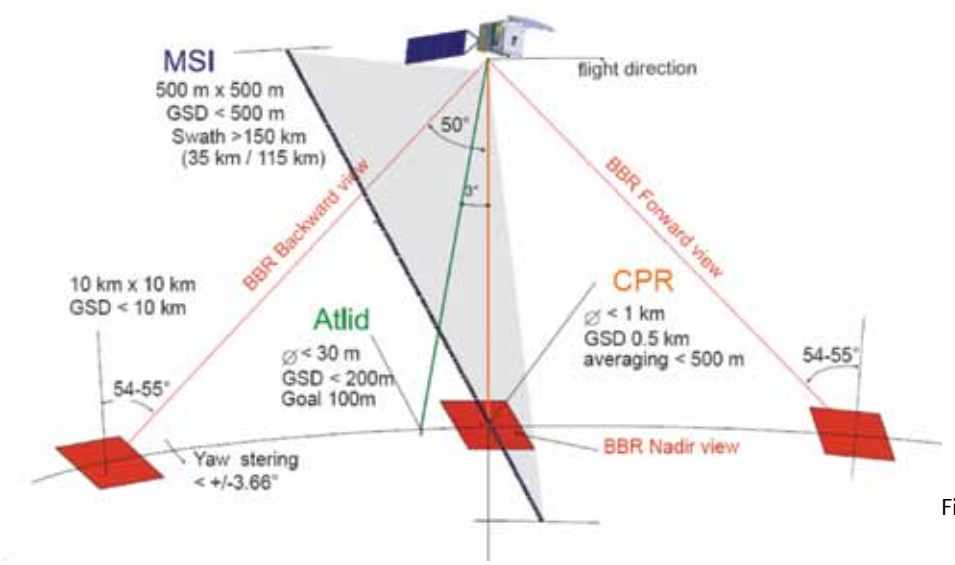

Fig. 3c1: EarthCARE observational concept

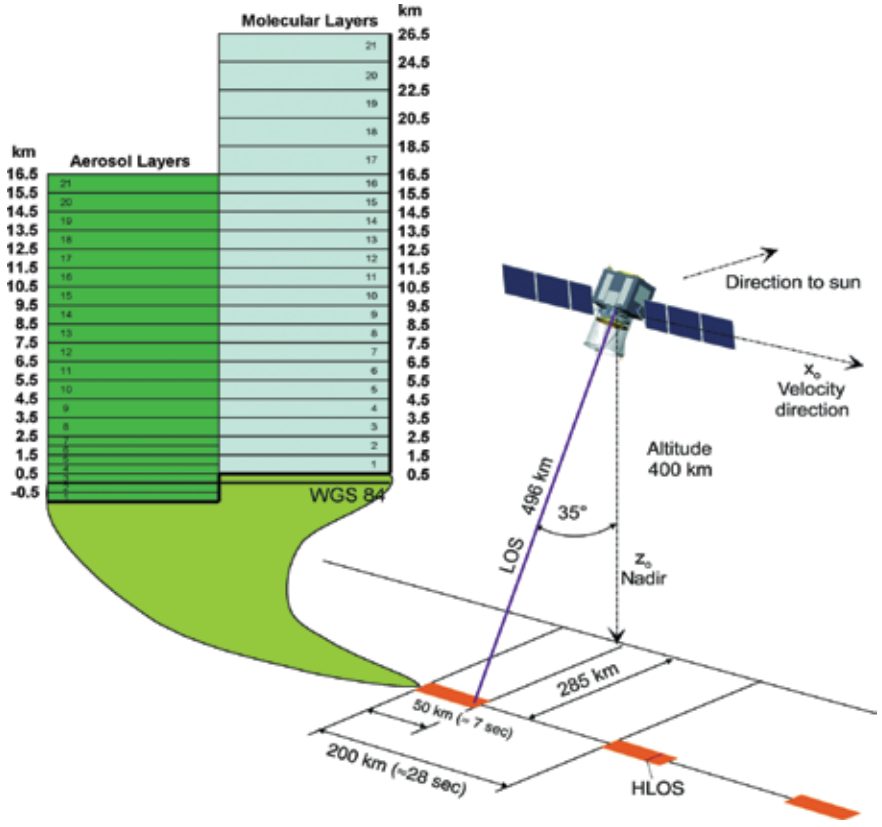

Fig. 3c2: ADM-Aeolus observation concept.

Operational Missions

The value of the current operational satellites systems, both geostationary (Meteosat Second Generation – MSG) and polar-orbiting (the European Polar System – EPS) has been clearly demonstrated, specifically with the capability to provide imagery products and estimates of ash extent, SO2, cirrus and ice.

These capabilities will be enhanced with the launch of the next generation of European operational satellites (Meteosat Third Generation - MTG and polar-orbiting satellites (the European Polar System Second Generation – EPS-SG)

The MTG system will comprise two satellites: an imaging platform (to be launched in ~2017), carrying the Flexible Combined Imager (FCI), the Lightening Imager (LI), the data collection system and search and rescue; and a sounding platform (to be launched in ~2019) carrying the InfraRed Sounder (IRS) and the GMES Sentinel 4 Ultraviolet Visible Near-infrared sounder (UVN).

The imagery, cloud, SO2 and ash products anticipated from the MTG-FCI will be available with improved spatial (1-2 km) and temporal (10mins) resolution as compared to MSG, and the aerosol detection capabilities will be enhanced with the inclusion of the 0.444 micron and 0.51 micron bands. Additionally the MTG-IRS (with heritage from the EPS/Metop IASI instrument) will provide improved ash detection capabilities with high temporal resolution (~30 minutes over Europe). However unlike IASI, it will not provide information on SO2. The Sentinel4 UVN will however provide estimates of SO2 at ~8km spatial resolution and 1 hour temporal resolution over the European domain. Information on aerosol optical depth and an absorbing aerosol index will also be provided.

In addition to the operational geostationary missions, the next generation of operational polar orbiting satellites is currently being planned. Missions under consideration include an imaging mission (VII) with similar capabilities for aerosol detection to MODIS, providing aerosol optical depth information at high spatial resolution, an infrared sounding mission (IRS), with enhanced spectral and radiometric performance as compared to EPS/Metop IASI, which will provide improved detection of ash, SO2, cirrus and ice, and the Sentinel 5 UVNS which will continue the aerosol optical depth and absorbing aerosol index measurements provided by GOME-2/SCIAMACHY and OMI but with significantly improved spatial resolution. Also under consideration is a multi-angle, multi-polarisation, multi-spectral instrument (3MI) (similar in concept to POLDER) which if realised will provide targeted aerosol information (including information on aerosol optical depth, coarse/fine mode, size, refractive index, height).

Other operational missions of relevance include the GMES Sentinel 2 and 3 missions targeting ocean and global land monitoring. In addition to ocean and land products, aerosol optical depth can also be provided.

Table 3c1: Satellite missions planned for Europe and ability to derive relevant data for volcanic plume monitoring (name, SO2 detection, Ash detection, Spatial Coverage and Launch status)

Instrument/Satellite	SO_2	Ash	Spatial coverage	Status and launch date
IASI/MetopB	Total column + altitude +-2 km Detection limit 2 DU	Estimated concentration (needs altitude assumption)	Polar (9:30; 21:30) Pixel 12 km	Phase C 2012
GOME2/MetopB	Total column + altitude Detection limit 2 DU	AAI[1], AOD[2]	Polar (9:30) Pixel 40x80 km^2	Phase C 2012
IASI/MetopB	Total column + altitude +-2 km Detection limit 2 DU	Estimated concentration (needs altitude assumption)	Polar (9:30; 21:30) Pixel 12 km	Phase C 2017
GOME2/MetopB	Total column + altitude Detection limit 2 DU	AAI, AOD	Polar (9:30) Pixel 40x80 km^2	Phase C 2017
Sentinel-Precursor Tropomi (OMI heritage)	Total column + altitude Detection limit 1 DU	AAI, AOD	Polar (13 :30) Pixel 7x7 km^2	Phase B 2014
Imagers/MTG (Severi heritage)	IR UTLS	IR ash concentration	GEO Full disk	Phase A 2017
IRS/MTG (IASI heritage, coarser spectral res.)	Only the n_1 band – low altitude detection only	Estimated concentration (needs altitude assumption)	GEO Full disk, pixel 4 km 30/60 min	Phase A 2019
UVS/MTG (Sentinel 4) (GOME2-OMI heritage)	Total column + altitude Detection limit 1 DU	AAI, AOD	GEO 25°W-30°E/ 25°N-60°N 10/20 min Pixel 8x8 km^2	Phase A 2019
IASI-NG/Post-EPS (IASI heritage, better spectral res.)	Total column + altitude +-1 km Detection limit 1 DU	Estimated concentration (needs altitude assumption)	Polar (9:30; 21:30) Pixel 12 km	Phase 0 2010
UVS/Post-EPS (Sentinel 5) GOME2 heritage	Total column + altitude Detection limit 1 DU	AAI, AOD	Polar (9 :30) Pixel 7x7 km^2	Phase 0 2010
3MI/Post-EPS (Polder- Parasol heritage)	-	AOD, Coarse/fine mode, size, refractive index, height	Polar (9 :30) Pixel 4km	Phase 0 2010

1 AAI= Absorbing Aerosol Index 2 AOD= Aerosol Optical Depth

References

Barton IJ, Prata AJ, Watterson IG, Young SA (1992) Identification of the Mount Hudson volcanic cloud over SE Australia. Geophys Res Lett 19:1211–1214

Bernard A, Rose WI (1984) The injection of sulfuric acid aerosols in the stratosphere by the El Chichon volcano and its related hazards to the international air traffic. Nat Hazards 3(1):59–67. doi:10.1007/ BF00144974

Bluth GJS, Schnetzler CC, Krueger AJ, Walter LS (1993) The contribution of explosive volcanism to global atmospheric sulphur dioxide concentrations. Nature 366:327–329

Carn SA, Krueger AJ, Krotkov NA, Gray MA (2004) Fire at Iraqi sulfur plant emits SO2 clouds detected by Earth Probe TOMS. Geophys Res Lett 31:L19105. doi:10.1029/2004GL020719

Carn SA, Krotkov NA, Yang K, Hoff RM, Prata AJ, Krueger AJ, Loughlin SC, Levelt PF (2007) Extended observations of volcanic SO2 and sulphate aerosol in the stratosphere. Atmos Chem Phys Discuss 7:2857–2871

Carn SA, Prata AJ, Karlsdottir S (2008) Circumpolar transport of a volcanic cloud from Hekla (Iceland). J Geophys Res 113. doi:10.1029/2008JD009878

Casadevall TJ (1994) The 1989/1990 eruption of Redoubt Volcano Alaska: impacts on aircraft operations. J Volcanol Geotherm Res 62(30):301–316

Casadevall TJ, Delos Reyes PJ, Schneider DJ (1996) The 1991 Pinatubo eruptions and their effects on aircraft operations. In: Newhall CG, Punongbayan RS (eds) Fire and mud: eruptions and lahars of Mount Pinatubo, Philippines. Philippines Institute of Volcanology and Seismology, Quezon City, University of Washington Press, Seattle, pp 625–636

Clerbaux C, Hadji-Lazaro J, Turquety S, George M, Coheur P-F, Hurtmans D, Wespes C, Herbin H, Blumstein D, Tournier B, Phulpin T (2007) The IASI/MetOp I mission: first observations and high- lights of its potential contribution to GMES. COSPAR Inf Bull 2007:19–24

Constantine EK, Bluth GJS, Rose WI (2000) TOMS and AVHRR sensors applied to drifting volcanic clouds from the august 1991 eruptions of Cerro Hudson. In: Mouginis-Mark P, Crisp J, Fink J (eds) AGU Monograph 116—Remote Sensing of Active Volcanism, pp 45–64

Eckhardt S, Prata AJ, Seibert P, Steibel K, Stohl A (2008) Estimation of the vertical profile of sulfur dioxide injection into the atmosphere by a volcanic eruption using satellite column measurements and inverse transport modeling. Atmos Chem Phys Discuss 8:3761–3805

Eisinger M, Burrows JP (1998) Tropospheric sulfur dioxide observed by the ERS-2 GOME instrument. Geophys Res Lett 25(22):4177–4180

Ellrod GP, Connell BH, Hillger DW (2003) Improved detection of airborne volcanic ash using multispectral infrared satellite data. J Geophys Res 108(D12):4356. doi:10.1029/2002JD002802

Fleming EL, Chandra S, Shoeberl MR, Barnett JJ (1988) Monthly mean global climatology of temperature, wind, geopotential height and pressure for 0–120 km. National Aeronautics and Space Administration, Technical Memorandum 100697, Washington, DC

Guffanti M, Albersheim S (2008) The United States national volcanic ash operations plan for aviation. Nat Hazards Special Issue: Aviation hazards from volcanoes. doi:10.1007/s11069-008-9247-1

Hanstrum BN, Watson AS (1983) A case study of two eruptions of Mount Galunggung and an investigation of volcanic eruption cloud characteristics using remote sensing techniques. Aust Meteorol Mag 31:131–177

Hillger DW, Clark JD (2002a) Principal component image analysis of MODIS for volcanic ash. Part I: most important bands and implications for future GOES imagers. J Appl Meteorol 41:985–1001

Hillger DW, Clark JD (2002b) Principal component image analysis of MODIS for volcanic ash. Part II: simulation of current GOES and GOES-M imagers. J Appl Meteorol 41:1003–1010

Holasek RE, Rose WI (1991) Anatomy of 1986 Augustine volcano eruptions as recorded by multispectral images processing of digital AVHRR weather satellite data. Bull Volcanol 53:42–435.

Holasek RE, Woods AW, Self S (1996) Experiments on gas-ash separation processes in volcanic umbrella clouds. J Volcanol Geotherm Res 70:169–181.

Krotkov NA, Carn SA, Krueger AJ, Bhartia PK, Yang K (2006) Band residual difference algorithm for retrieval of SO2 from the Aura Ozone Monitoring Instrument (OMI). IEEE Trans Geosci Remote Sens 44(5):1259–1266.

Krueger AJ (1983) Sighting of El Chichon sulfur dioxide clouds with the nimbus 7 total ozone mapping spectrometer. Science 220:1377–1379.

Krueger AJ, Walter LS, Bhartia PK, Schnetzler CC, Krotkov NA, Sprod I, Bluth GJS (1995) Volcanic sulfur dioxide measurements from the total ozone mapping spectrometer instruments. J Geophys Res 100(D7):14057–14076.

Krueger AJ, Schaefer SJ, Krotkov N, Bluth GJS, Baker S (2000) Ultraviolet remote sensing of volcanic emissions. In: Mouginis-Marks PJ, Crisp JA, Fink JH (eds) Remote sensing of active volcanism. Geophys Monogr Ser 116:2543, AGU, Washington, DC.

Malingreau J, Kaswanda P (1986) Monitoring volcanic eruptions in Indonesia using weather satellite data: the Colo eruption of July 28, 1983. J Volcanol Geotherm Res 27(1–2):179–194.

Matson M (1984) The 1982 El Chichon volcano eruptions—a satellite perspective. J Volcanol Geotherm Res 23:1–10.

Miller TP, Casadevall TJ (1999) Volcanic ash hazards to aviation. In: Sigurdsson H, Houghton B, McNutt SR, Ryman H, Stix J (eds) Encyclopedia of volcanoes. Academic Press, San Diego, pp 915–930.

Mosher FR (2000) Four channel volcanic ash detection algorithm, Preprint Volume. 10th Conference on Satellite Meteorology and Oceanography, Long Beach, California, 9–14 January, 2000, pp 457–460.

Pavolonis MJ, Feltz WF, Heidinger AK, Gallina GM (2006) A daytime complement to the reverse absorption technique for improved automated detection of volcanic ash. J Atmos Oceanic Technol 23:1422–1444.

Pergola N, Tramutoli V, Marchese F, Scaffidi I, Lacav T (2004) Improving volcanic ash cloud detection by a robust satellite technique. Remote Sens Environ 90:1–22.

Pieri D, Ma C, Simpson JJ, Hufford G, Grindle T, Grove C (2002) Analyses of in-situ airborne ash from the February 2000 eruption of Hekla volcano, Iceland. Geophys Res Lett 29:16. doi:10.1029/2001GL013688.

Prata AJ (1989a) Observations of volcanic ash clouds using AVHRR-2 radiances. Int J Remote Sens 10(4–5):751–761.

Prata AJ (1989b) Radiative transfer calculations for volcanic ash clouds. Geophys Res Lett 16(11): 1293–1296.

Prata AJ, Grant IF (2001) Retrieval of microphysical and morphological properties of volcanic ash plumes from satellite data: application to Mt. Ruapehu, New Zealand. Q J R Meteorol Soc 127(576B): 2153–2179.

Prata AJ, Kerkmann J (2007) Simultaneous retrieval of volcanic ash and SO2 using MSG-SEVIRI mea- surements. Geophys Res Lett 34:L05813. doi:10.1029/2006GL028691.

Prata AJ, Bluth GJS, Rose WI, Schneider DJ, Tupper AC (2001) Comments on Failures in detecting volcanic ash from a satellite-based technique. Remote Sens Environ 78:341–346.

Prata, A. J., and Tupper, A. T., (2009) Aviation hazards from volcanoes: the state of the science, Nat Hazards doi: 10.1007/s11069-009-9415-y.

Prata AJ, Rose WI, Self S, O'Brien DM (2003) Global, long-term sulphur dioxide measurements from TOVS data: a new tool for studying explosive volcanism and climate. Volcanism and the Earth's atmosphere, geophysics monograph 139 AGU, pp 75–92.

Prata AJ, Carn SA, Stohl A, Kerkmann J (2007) Long range transport and fate of a stratospheric volcanic cloud from Soufriere ills volcano, Montserrat. Atmos Chem Phys 7:5093–5103.

Richardson AJ (1984) El Chichon volcanic ash effects on atmospheric haze measured by NOAA-7 AVHRR data. Remote Sens Environ 16:157–164.

Richter A, Wittrock F, Burrows JP (2006) SO2 measurements with SCIAMACHY. In: Proceedings of the first conference on atmospheric science, Frascati, Italy, 8–12 May 2006. ESA publication SP-628.

Rose WI, Delene DJ, Schneider DJ, Bluth GJS, Kruger AJ, Sprod I, McKee C, Davies HL, Ernst GJ (1995) Ice in the 1994 Rabaul eruption: implications for volcanic hazard and atmospheric effects. Nature 375:477–479.

Sawada Y (1987) Study on analysis of volcanic eruptions based on eruption cloud image data obtained by the Geostationary Meteorological Satellite (GMS). Technical reports of the Meteorological Research Institute, vol 22, 335 pp.

Sawada Y (1996) Detection of explosive eruptions and regional tracking of volcanic ash clouds with geostationary meteorological satellites (GMS). In: Scarpa R, Tilling RI (eds) Monitoring and miti- gation of volcano hazards. Springer-Verlag, Berlin, Heidelberg, pp 299–314.

Schneider DJ, Rose WI, Kelley L (1995) Tracking of 1992 eruption clouds from Crater Peak of Mount Spurr volcano, Alaska, using AVHRR. US Geol Surv Bull 2139:27–36.

Schneider DJ, Rose WI, Coke LR, Bluth GJS (1999) Early evolution of a stratospheric volcanic eruption cloud as observed with TOMS and AVHRR. J Geophys Res 104(D4):4037–4050.

Simkin T, Seibert L (1994) Volcanoes of the world, 2nd edn. Geoscience Press, Tucson Simpson JJ, Hufford G, Pieri D, Berg J (2000) Failures in detecting volcanic ash from a satellite-based technique. Remote Sens Environ 72:191–217.

Simpson JJ, Hufford G, Pieri D, Servranckx R, Berg J (2002) The february 2001 eruption of Mount Cleveland, Alaska: case study of an aviation hazard. Weather Forecast 17:691–704.

Thomas W, Erbertseder T, Ruppert T, Van Roozendael M, Verdebout J, Balis D, Meleti C, Zerefos C (2004) On the retrieval of volcanic sulfur dioxide emissions from GOME backscatter measurements. J Atmos Chem 50:295–320. doi:10.1007/s10874-005-5079-5.

Torres O, Bhartia PK, Herman JR, Ahmad Z, Gleason J (1998) Derivation of aerosol properties from satellite measurements of backscattered ultraviolet radiation: theoretical basis. J Geophys Res, 103(D14):17099–17110.

Tupper A, Carn SA, Davey J, Kamada Y, Potts RJ, Prata AJ, Tokuno M (2004) An evaluation of volcanic cloud detection techniques during recent significant eruptions in the western ring of fire. Remote Sens Environ., 91:27–46.

Urai M (2004) Sulfur dioxide flux estimation from volcanoes using advanced spaceborne thermal emission and reflection radiometer—a case study of Miyakejima volcano, Japan. J Volcanol Geotherm Res., 134(1–2):1–13.

Van Geffen J, Van Roozendael M, Di Nicolantonio W, Tampellini L, Valks P, Erbetseder T, Van der A (2007) Monitoring of volcanic activity from satellite as part of GSE PROMOTE. Proceedings of the first conference on atmospheric science, Frascati, Italy, 8–12 May 2006. ESA publication SP-628.

Watkin SC (2003) The application of AVHRR data for the detection of volcanic ash in a volcanic ash advisory centre. Meteorol Appl 10:301–311.

Wen S, Rose WI (1994) Retrieval of sizes and total masses of particles in volcanic clouds using AVHRR bands 4 and 5. J Geophys Res 99(D3):5421–5431.

Witham CS, Hort MC, Potts R, Servranckx R, Husson P, Bonnardot F (2007) Comparison of VAAC atmospheric dispersion models using the 1 November 2004 Grimsvtn eruption. Meteorol Appl 14: 27–38.

Yu T, Rose WI, Prata AJ (2002) Atmospheric correction for satellite-based volcanic ash mapping and retrievals using split window IR data from GOES and AVHRR. J Geophys Res 107(D16):4311. doi:10.1029/2001JD000706.

An ESA Communications Production